Neuron

Article

A reciprocal glial circuit calibrates injury information and governs the tissue response balance

Graphical abstract

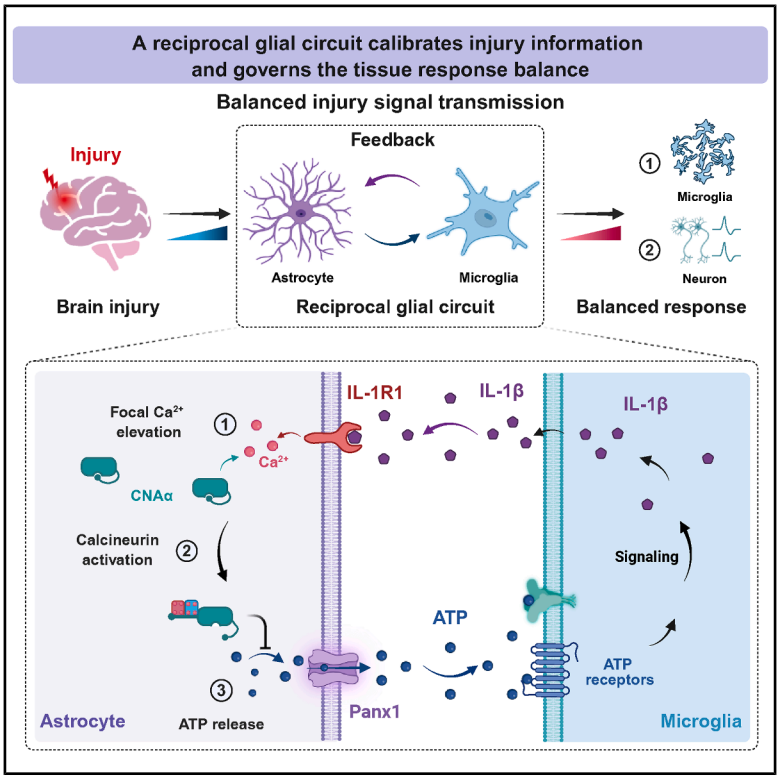

Highlights

- Brain calibrates acute injury by scaling ATP Inflares with injury severity
- Microglial IL-1β provides tunable feedback to regulate astrocytic ATP release
- Astrocytes coordinate injury and microglial feedback by Ca^{2+}-calcineurin pathway
- Disruption of the reciprocal glial circuit worsens early-stage injury outcomes

Authors

Pengwei Luan, Jianming Jia, Yue Chen, ..., Ya Wang, Ádám Dénes, Miao Jing

Correspondence

denes.adam@koki.hun-ren.hu (Á.D.), jingmiao@cibr.ac.cn (M.J.)

In brief

Brain injury responses must be carefully balanced to limit damage while enabling repair. Luan et al. show that astrocytes and microglia form a reciprocal signaling circuit and achieve balanced ATP release through microglial IL-1β-mediated negative feedback, allowing the brain to calibrate injury responses and initiate balanced tissue responses.

Luan et al., 2026, Neuron *114*, 1–14
September 2, 2026
https://doi.org/10.1016/j.neuron.2026.03.031

CellPress

Neuron

CellPress

Article

A reciprocal glial circuit calibrates injury information and governs the tissue response balance

Pengwei Luan,[1,2,3] Jianming Jia,[2,3,4] Yue Chen,[2,3] Fengxue Xi,[2,3,5] Anett D. Schwarcz,[6,7] Xiujie Jiang,[2,3] Zsuzsanna Környei,[6] Balázs Kalmár,[6] Ya Wang,[2,3] Ádám Dénes,[6,*] and Miao Jing[1,2,3,8,*]

[1]Academy for Advanced Interdisciplinary Studies, Peking University, Beijing 100871, China
[2]Beijing Institute for Brain Research, Chinese Academy of Medical Sciences & Peking Union Medical College, Beijing 102206, China
[3]Chinese Institute for Brain Research, Beijing 102206, China
[4]College of Biological Science, China Agricultural University, Beijing 100193, China
[5]Basic Medical Sciences, Capital Medical University, Beijing 100069, China
[6]Momentum Laboratory of Neuroimmunology, HUN-REN Institute of Experimental Medicine, Budapest 1083, Hungary
[7]János Szentágothai Doctoral School of Neurosciences, Schools of PhD Studies, Semmelweis University, Budapest 1085, Hungary
[8]Lead contact
*Correspondence: denes.adam@koki.hun-ren.hu (Á.D.), jingmiao@cibr.ac.cn (M.J.)
https://doi.org/10.1016/j.neuron.2026.03.031

SUMMARY

Brain injury elicits complex tissue responses that are dynamically regulated between activation and resolution, yet the mechanisms that govern this balance remain elusive. We show that acute injury evokes focal extracellular ATP events (Inflares) with characteristic spatiotemporal signatures that scale quantitatively with injury severity, suggesting a glial mechanism for damage calibration. We further reveal that microglia exert negative feedback on Inflares by tuning interleukin (IL)-1β output based on extracellular ATP levels and cellular state. The IL-1β signal is directly received by astrocytes through IL-1R1 and intracellular Ca^{2+}-calcineurin signaling, where it converges with injury input to shape Panx1-dependent ATP release. These bidirectional interactions form a reciprocal glial circuit that enforces a balanced injury response, while disrupting the circuit destabilizes the dynamic control, impairing the cellular reactivity and worsening early injury outcomes. Our findings uncover a glial circuit and molecular players that dynamically regulate tissue injury responses.

INTRODUCTION

Central nervous system (CNS) injuries are a leading cause of chronic disability and death worldwide.[1] Upon acute injury, the brain initiates complex pathological cascades, including cellular activation, inflammatory signaling, and tissue remodeling, yet their uncontrolled amplification or persistence may disrupt tissue integrity, leading to secondary damage and long-term dysfunction.[2] These observations raise the fundamental question of how injury responses, including their magnitude, timing, and spatial profile, are calibrated to match the extent of damage and ensure appropriate reactivity.

Astrocytes and microglia are uniquely positioned to sense and integrate injury cues and shape downstream responses. Astrocytes respond to diverse stimuli and release messengers to modulate the local immune environment or form glial scars that prevent the spread of damage.[3,4] Microglia, as the resident brain immune cells, rapidly sense injury-induced changes and orchestrate inflammation through cytokine production as well as clear cellular debris by phagocytosis.[5] Emerging evidence suggests that glial cells communicate bidirectionally through chemical signals to form regulatory networks[6–8]; however, the mechanisms and their contribution to injury responses remain unclear.

Extracellular ATP is a pivotal glial messenger that orchestrates cellular communication and modulates injury responses.[9–11] With the development of genetically encoded sensors, the spatiotemporally selective ATP events termed Inflares were recently identified as an active form of ATP release from astrocytes following injury, extending the role of ATP as a damage-associated molecular pattern (DAMP) from dying cells to an active, structured signal that transmits injury information.[12] However, how these signals are controlled to ensure proportional injury responses remains unknown. Here, using graded *in vivo* laser injury models, we map a quantitative relationship between lesion severity and astrocytic Inflare properties, reflecting the balanced internal response to injury. Through molecular screening and cell-type-specific genetic manipulations, we discover a reciprocal microglia-astrocyte feedback circuit in which the microglia-derived cytokine interleukin (IL)-1β directly stimulates the astrocytic IL-1 receptor 1 (IL-1R1) and engages

Please cite this article in press as: Luan et al., A reciprocal glial circuit calibrates injury information and governs the tissue response balance, Neuron (2026), https://doi.org/10.1016/j.neuron.2026.03.031

intracellular Ca^{2+}-calcineurin signaling to suppress Panx1-dependent ATP release. Importantly, disruption of this circuit destabilizes injury balance and unleashes excessive ATP signals, driving maladaptive microglial behaviors, impaired neural network recovery, and worsened early injury outcomes.

RESULTS

A quantitative scaling of Inflares with injury supports a balanced injury response

To test whether injury responses are calibrated to damage severity, we used Inflares as a quantitative readout and examined how their properties scale with injury. Awake mice expressing the ATP1.0 sensor in astrocytes were subjected to different intensities of focal laser ablations (FLAs) in the visual cortex, which generated graded lesions whose areas were quantified as an index of injury severity (Figure 1A). The spatiotemporal distributions of Inflares were monitored before and at multiple time points after injury. Individual Inflares were illustrated in two complementary ways: a spatial region of interest (ROI) map with the temporal projection of signals, and the temporal distribution of events as a bar plot with the height and width of the bar encoding Inflare amplitude and duration, respectively (Figure S1A). At both 0.5 and 2 h after injury, we observed a robust elevation in Inflare frequency over baseline, which was in direct proportion to lesion size (Figures 1B–1D; $R^2 = 0.81$, $p < 0.001$). Notably, the single-event properties of Inflares, including their size and duration, remained constant across different injuries (Figures S1B and S1C), consistent with the population coding of Inflares as recently reported.[12] The baseline Inflares detected prior to laser injury likely reflect residual effects of surgical preparation, as their frequency was reduced under thinned-skull cranial window conditions, which are associated with less tissue disturbance (Figure S1D).[13]

At the population level, Inflares exhibited characteristic temporal decay and spatial distribution that carry injury information, suggesting that these properties may also be under tight control. Indeed, quantifying Inflares over time revealed a steeper decline following severe injuries, with the decay rate scaling linearly with injury severity (Figure 1E). By 7 days after acute injury, Inflare frequency returned to baseline levels, suggesting that the response predominantly occurs during the early phase following injury (Figure S1E). Similarly, the spatial gradient in population Inflares could be quantitatively described as the decrease of event density away from the injury center, in which the spatial decay slope increased linearly with the injury severity (Figure 1F), together supporting the balanced regulation of Inflares at both temporal and spatial scales. Randomly shuffling the pairing between injury and Inflare abolished correlations in each dimension (Figure S1F). Altogether, these data suggest that multiple dimensions of the Inflare scale with injury severity, pointing to a glia-dependent mechanism that regulates injury responses.

Feedback inhibition by microglia is required for balanced injury responses

Having established the quantitative relationship between injury and Inflares, we next explored the mechanisms that enforce the balance. Using transgenic mice, we validated that injury-evoked Inflares predominantly originate from astrocytes and are gated by Panx1 (Figure S1G).[12] As robust control systems typically employ negative feedback to counteract perturbations,[14] we hypothesized that microglia, which are equipped with purinergic receptors to sense ATP and with molecular machineries to shape astrocytic reactivity,[15] might function as a regulatory node to modulate astrocytic responses. We established experimental conditions in which microglia were either depleted by continuous administration of CSF1R inhibitor (BLZ945 for 2 weeks) or repopulated over a further 2 weeks after drug withdrawal, followed by the comparison of FLA-evoked Inflares across conditions (Figure 1G, left). Immunofluorescence staining validated > 99% depletion of microglia and > 87% repopulation efficiency and its cell-type specificity (Figures 1G, right, and S2A–S2D). Strikingly, microglial depletion led to pronounced elevation in Inflare frequency (Figure 1H; Video S1), as well as recurrent Inflares from the same spatially defined ROIs (Figures 1I and S2E–S2H). Moreover, the decline in Inflare frequency after injury was slowed down over 24 h, indicating the altered injury response at the temporal scale (Figures S2I and S2M). Individual Inflares also became spatially broader and temporally prolonged, suggesting a loss of spatiotemporal precision in extracellular ATP signaling (Figures S2J–S2L and S2N–S2P). Microglia depletion also led to increased variability in the linear scaling between Inflare frequency and injury severity (Figure 1J). Remarkably, microglial repopulation largely restored Inflare dynamics and stabilized their linear relationship with injury. The microglia-dependent phenotype was consistent in both male and female mice, implying a gender-independent mechanism (Figure S2). Together, the presence of microglia provides critical feedback inhibition that balances astrocytic ATP release following acute brain injury.

Given that ectonucleotidases CD39 and CD73 critically contribute to extracellular ATP signaling,[16] we next examined whether changes in these enzymes may explain the loss of balance accompanied by microglia depletion (Figure S3A). In CD39 knockout (KO) mice, FLA-evoked Inflares exhibited increased size and duration, partially resembling the phenotype in microglia-depleted mice, whereas CD73 knockout had a negligible effect (Figures S3B–S3E). However, neither CD39 nor CD73 knockout recapitulated the rise in Inflare frequency observed with microglia depletion (Figure S3F), the key coding dimension of injury information. These results argue against ATP degradation as the primary feedback mechanism and instead suggest an upstream signal that selectively modulates astrocytic ATP outputs.

Microglia integrate activation state and extracellular ATP signals to modulate feedback inhibition

Recent single-cell sequencing studies have revealed that microglia adopt diverse and context-dependent states, suggesting they may integrate environmental and functional needs to adjust their outputs.[17,18] We found that Inflares occur within hours post injury that precede the appearance of $CD11c^+$ (a marker of disease-associated microglia) microglia in our model[19,20] (Figures S3G and S3H). We next employed two complementary genetic approaches to modulate microglia states and tested whether microglial feedback exhibits state-dependency. First, we employed transgenic mice to eliminate microglial P2Y12 receptors that are critical in shaping their state, reactivity, and

Please cite this article in press as: Luan et al., A reciprocal glial circuit calibrates injury information and governs the tissue response balance, Neuron (2026), https://doi.org/10.1016/j.neuron.2026.03.031

CellPress

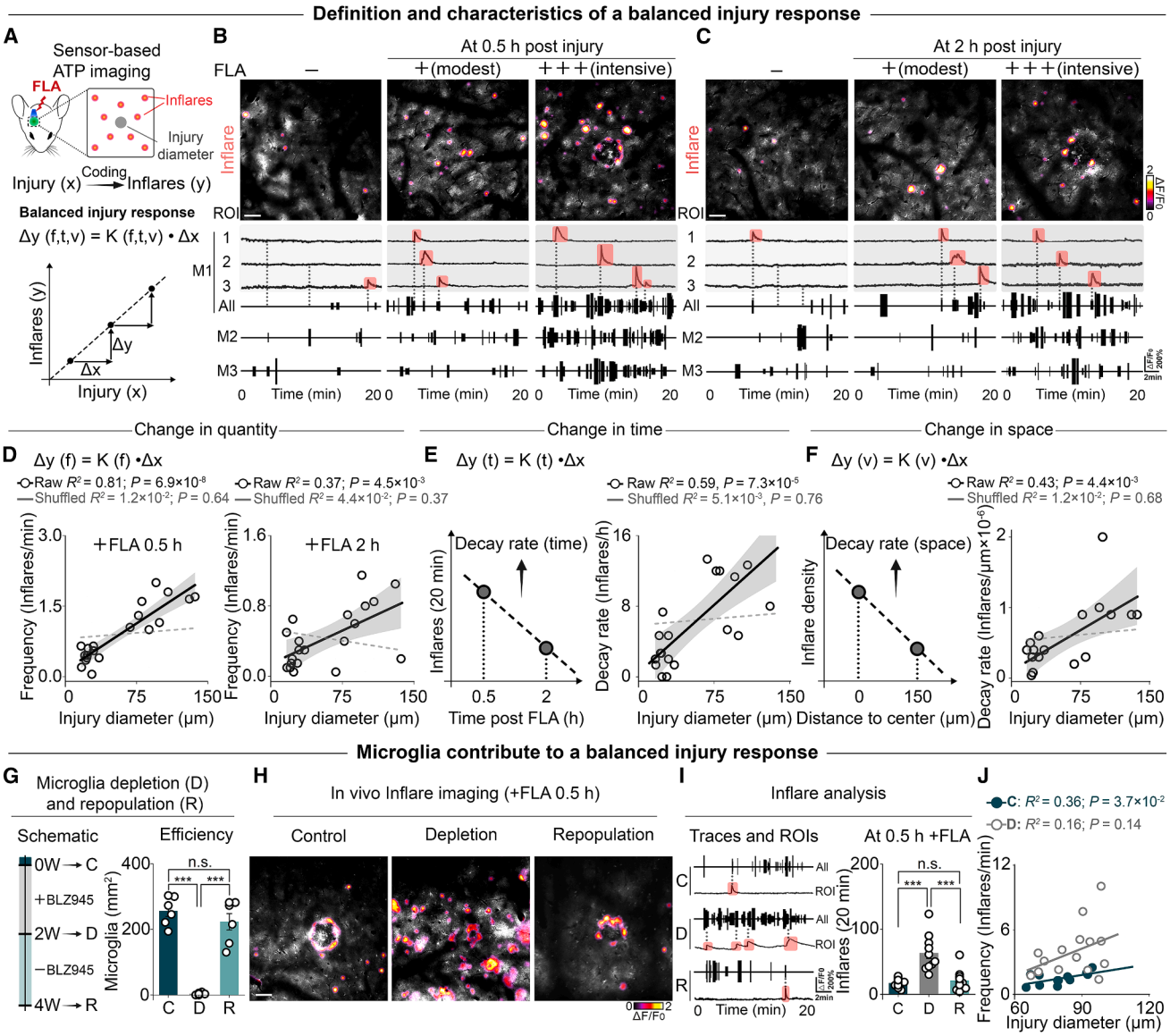

Figure 1. A balanced injury response and its maintenance by microglia

(A) Top, awake mice were subjected to different intensities of focal laser injuries (FLA), and extracellular ATP dynamics (Inflares) were monitored by the astrocytic-expressing ATP1.0 sensor. Bottom, conceptual model depicting a balanced injury response in which changes in ATP Inflares (y)—including their frequency (f), temporal (t), and spatial (v) distributions—scale linearly with injury severity (x).

(B) Representative images (top) and traces (bottom) showing Inflares before (–) and at 0.5 h after modest (+) and intensive (+++) FLA injuries. Images represent the projection of all Inflares over time (20 min), while temporal traces represent the projection of Inflares over space. Fluorescence responses from three Inflare ROIs in mouse 1 (M1) are shown and are aligned with their positions in the temporal traces.

(C) Similar to (B), except the recordings were conducted at 2 h after injuries.

(D) Quantitative analysis of correlation between Inflare frequency and injury diameter at 0.5 h (left) and 2 h (right) post injury (0.5 h: $n = 11$ mice [+], $n = 9$ mice [+++]; $p = 6.92 \times 10^{-8}$; 2 h: $n = 11$ mice [+], $n = 9$ mice [+++]; $p = 4.50 \times 10^{-3}$). Linear fittings for shuffled data are shown.

(E) Left, schematic representation of the temporal decay of Inflare frequencies after injury. Right, quantitative analysis of the correlation between the Inflare decay rate and injury diameter ($n = 20$ mice; $p = 7.33 \times 10^{-5}$).

(F) Similar to (E), except the decay rate of Inflare density in the area away from the injury center is analyzed ($n = 17$ mice; $p = 4.39 \times 10^{-3}$).

(G) Left, schematic for microglial depletion and repopulation by continuous application or withdrawal of the CSF1R inhibitor BLZ945 (C, control; D, depletion; and R, repopulation). Right, the quantification of microglia density in each condition ($n = 6$ mice; $p = 2.97 \times 10^{-5}$ for C and D; $p = 4.68 \times 10^{-4}$ for D and R; and $p = 0.34$ for C and R).

(H) Representative images showing FLA-evoked Inflares under different microglial manipulation conditions.

(I) Representative ROIs of Inflares in each condition (left) and total Inflares (in 20 min recording) at 0.5 h after FLA injuries ($n = 12/10/12$ mice for C/D/R, respectively; $p = 5.16 \times 10^{-4}$ for C and D; $p = 2.09 \times 10^{-4}$ for D and R; and $p = 0.44$ for C and R).

(legend continued on next page)

Please cite this article in press as: Luan et al., A reciprocal glial circuit calibrates injury information and governs the tissue response balance, Neuron (2026), https://doi.org/10.1016/j.neuron.2026.03.031

morphology (Figures 2A, 2B, and S4A–S4E).[10,21] Compared with wild-type (WT) controls, P2Y12-deficient mice exhibited persistently elevated Inflares over 12 h after injury (Figures 2C and 2D; Video S2), mirroring the microglia-depleted mice and indicating attenuated feedback inhibition. In an alternative setting, we chemogenetically manipulated microglia in a temporally controllable manner using our recently developed microglial expression of the designer receptors exclusively activated by designer drugs (microDREADD) mouse line.[22] Chemogenetic priming of microglia has been validated to induce rapid Ca^{2+} elevation and phenotypic remodeling of microglia (Figures S4F–S4H),[22,23] as well as the release of inflammatory cytokines.[24] As controls, transgenic mice with microglia-specific expression of the red fluroscent protein (RFP) mScarlet were generated and referred to as microRFP mice (Figures 2E and 2F).[25] Upon injury, mice in which microglia were chemogenetically stimulated with clozapine N-oxide (CNO) exhibited a remarkable reduction in both the frequency and persistence of Inflares compared with saline-treated controls, an effect not observed in microRFP mice (Figures S5A–S5F; Video S3). Replacing the stimulator with deschloroclozapine (DCZ) with higher potency and selectivity also led to similar results (Figures S5G–S5I), indicating the elevated feedback inhibition when microglia are chemogenetically activated. With the altered feedback, the population Inflares decreased their linear scaling with injury, which further supports the importance of microglial feedback in governing the balanced response (Figures 2G and 2H). Notably, neither P2Y12 deficiency nor chemogenetic modulation altered individual Inflare properties (Figures S5J and S5K), suggesting targeted feedback on the coding dimension of Inflares.

We next explored whether microglia adjust their feedback strength to varying ATP inputs (Figure 2I, left), thereby forming a reciprocal circuit, or they simply provide constant feedback as a gain control (Figure 2I, right). We adjusted the injury intensities to generate varied Inflare frequencies (input) and quantified feedback strength (output) using a microglial feedback index (MFI), defined as the relative increase in Inflare frequency upon microglia depletion (Figure 2J; see STAR Methods for details). If feedback was constant, microglia depletion would cause a uniform increase in Inflares across all injury levels. Instead, we observed a disproportionately greater increase following high-intensity injury, deviating from the parallel scaling that supports the tunable feedback from microglia (Figure 2K). Quantitative analysis further confirmed a linear relationship between input (Inflares) and MFI (output), indicating that microglia dynamically sense ATP levels to adjust feedback strength (Figure 2L). Overall, our results show that microglial feedback inhibition is jointly shaped by extracellular ATP signals and microglial activation state, thereby closing a bidirectional glial circuit that governs injury balance.

Microglial feedback inhibition on Inflares is mediated by cytokine IL-1β

To identify the mediator of microglial feedback on ATP release, we reasoned that it should increase after injury and decrease upon microglial depletion (Figure 3A). We performed transcriptomic screening focused on secretory proteins across injury and microglial manipulation conditions. The analysis revealed several candidates, including IL-1β, IL-1α, and chemokine C-C motif ligand 2 (CCL2), all harboring corresponding receptors on astrocytes (Figures 3B and 3C). To functionally assess the potency of candidates, we set an *ex vivo* gain-of-function assay to apply individual candidates on acute brain slices and evaluated their effects on FLA-evoked Inflares (Figure S6A). Among these factors, only IL-1β robustly suppressed the Inflare frequency without altering their size and duration (Figures 3D, 3E, and S6B). The inhibitory effect of IL-1β was abolished by IL-1 receptor antagonist (IL-1ra), its neutralizing antibody (NAb), or its heat inactivation (Figure 3E), confirming the requirement of the functional IL-1β-IL-1R1 axis. Using a chemogenetic system where Inflares were robustly evoked from hM_3Dq-expressing astrocytes, we validated the inhibitory effect of IL-1β on Inflares and its dependence on IL-1R1 signaling (Figures 3F, 3G, S6C, and S6D). IL-1R1 inhibitor Anakinra was also effective in blocking the elevated feedback inhibition from DREADD-stimulated microglia (Figures S6E and S6F). Notably, a 5-min exposure to IL-1β was sufficient to suppress subsequent Inflares, suggesting rapid and transcription-independent IL-1R signaling.

To assess whether endogenous IL-1β mediates microglial feedback, we investigated if blocking IL-1β signaling *in vivo* would relieve the feedback inhibition. Systemic administration of the brain-penetrant IL-1R1 antagonist Anakinra[26] was sufficient to elevate the Inflare frequency throughout 12 h post injury (Figures 3H–3J). Increased Inflares by Anakinra were not observed in astrocytic-*Panx1* deficient mice (Figures S6G and S6H). Conversely, systemic intraperitoneal (i.p.) injection of IL-1β reduced the frequency and persistence of Inflares after FLA (Figures 3K–3M) in both wild-type and astrocytic Panx1-overexpression mice (Figures S7A–S7C). We further validated that co-culture of primary microglia and astrocytes significantly reduced ATP Inflares compared with astrocyte-only cultures (Figure S7D). IL-1β treatment also reduced extracellular ATP levels in cultured astrocytes detected by both the ATP1.0 sensor and luminescence assay, supporting a direct modulatory effect of IL-1β on astrocytic ATP release (Figures S7E–S7G).

If IL-1β is the primary effector driving feedback inhibition, its abundance should track the temporal dynamics of feedback after injury. To explore this, we extracted local tissues at different time points prior to or after injury and measured the IL-1β protein levels using ELISA (Figure 3N). Indeed, IL-1β progressively accumulated after injury, with its temporal pattern closely matching the MFI (Figure 3O), supporting its role as a tunable regulator of ATP release. These findings position IL-1β as a molecular linchpin in the microglia-astrocyte circuit that regulates injury balance.

Direct microglial IL-1β to astrocytic IL-1R1 signaling shapes injury balance

We next dissected the cellular source and target of IL-1β in the feedback regulation of Inflares (Figure 4A). Single-cell

(J) Quantitative correlation between injury diameters and Inflare frequencies in control (C) or microglia-depleted (D) mice.
Scale bars, 50 μm.
See also Figure S1 for details and Table S1 for statistics.

Please cite this article in press as: Luan et al., A reciprocal glial circuit calibrates injury information and governs the tissue response balance, Neuron (2026), https://doi.org/10.1016/j.neuron.2026.03.031

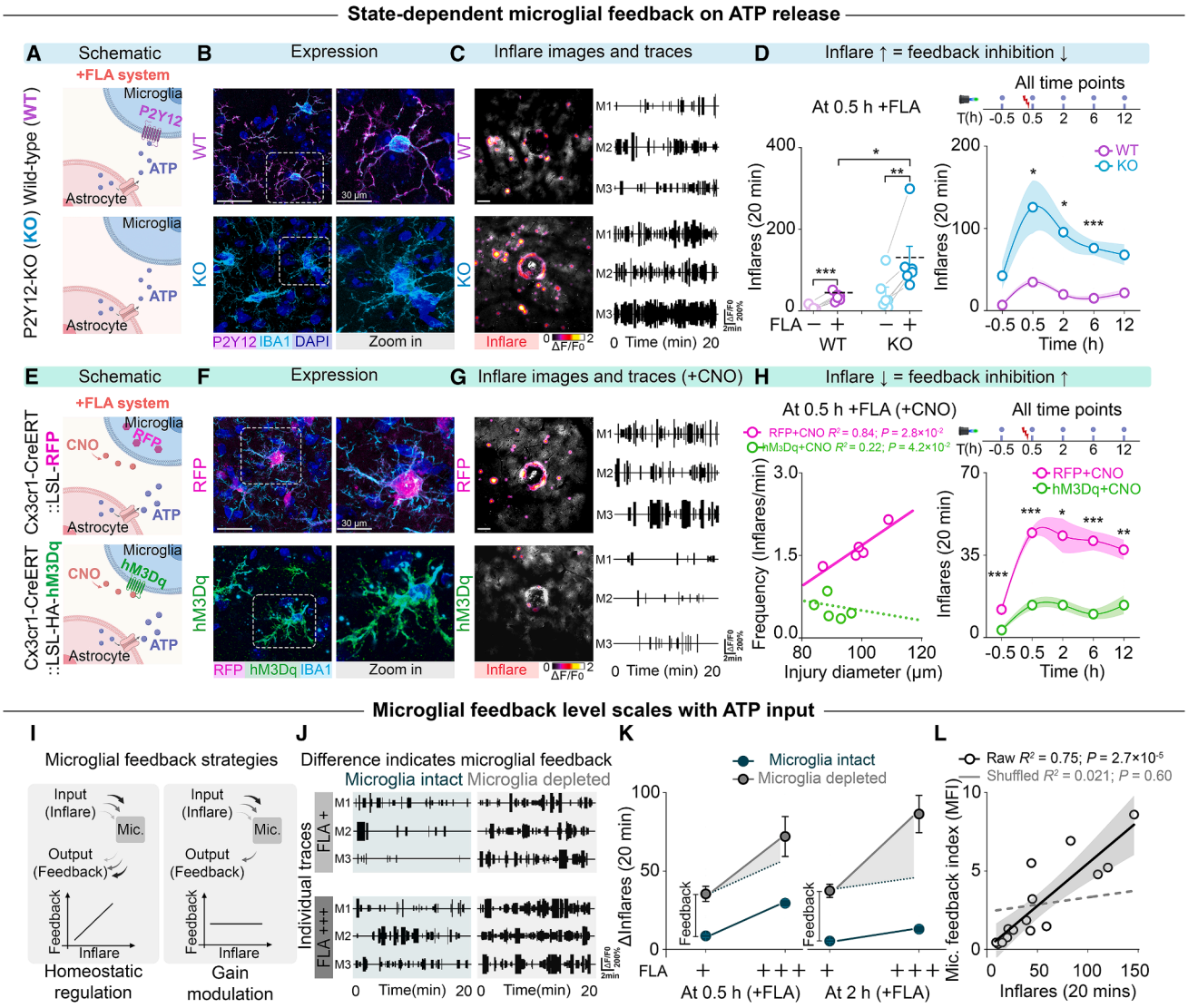

Figure 2. Microglia exert tunable and state-dependent feedback inhibition on Inflares

(A) Schematic showing the recording of FLA-evoked Inflares in wild-type (WT, top) and P2Y12 knockout (KO, bottom) mice.

(B) Immunofluorescence staining of P2Y12 (magenta) in microglia (IBA1, cyan).

(C) Representative images (left) and temporal distributions (right) of FLA-evoked Inflares in WT (top) and P2Y12 KO (bottom) mice at 0.5 h after FLA.

(D) Left, group analysis of Inflare frequency in WT and P2Y12 KO mice at 0.5 h after FLA (n = 6 mice; $p = 7.81 \times 10^{-5}$ in WT; $p = 8.30 \times 10^{-3}$ in KO; and $p = 4.93 \times 10^{-2}$ for +FLA between WT and KO). Right, time course of Inflare frequency changes in WT and P2Y12 KO mice ($p = 4.93 \times 10^{-2}$, 1.02×10^{-2}, and 1.20×10^{-4} for 0.5, 2, and 6 h, respectively).

(E–G) Similar to (A)–(C), except the experiments were performed in mice with microglial expression of RFP (top) or chemogenetic actuator hM_3Dq (bottom).

(H) Left, correlation between injury diameter and Inflare frequencies at 0.5 h post FLA in RFP and hM_3Dq mice (n = 5 mice per group). Right, time course of Inflare frequency changes (n = 5 mice; $p = 6.01 \times 10^{-4}$, 2.40×10^{-5}, 2.67×10^{-2}, 3.97×10^{-4}, and 8.90×10^{-3} for −0.5, 0.5, 2, 6, and 12 h, respectively). CNO (2 mg/kg i.p.) was administered 2 h before and 6 h after FLA.

(I) Schematics showing potential microglial feedback strategies.

(J) Temporal distributions of FLA-evoked Inflares in mice with intact microglia (left) and with microglia depleted (right) under varying FLA intensities.

(K) Group analysis of the FLA-evoked changes in Inflare frequency (ΔInflare) in mice with or without microglia. Microglial feedback level is indicated as the difference in Inflares between intact and depleted conditions, and the shaded area denotes deviation from a constant feedback (parallel to microglia-intact condition) (n = 11 mice [+] and 9 mice [+++] for intact; n = 12 mice [+] and 11 mice [+++] for depleted).

(L) Relationship between Inflare frequency and microglial feedback index (MFI). The linear fitting for shuffled data is shown (n = 15 mice, $p = 2.73 \times 10^{-5}$).

Scale bars, 50 μm.

See Table S1 for statistics.

Please cite this article in press as: Luan et al., A reciprocal glial circuit calibrates injury information and governs the tissue response balance, Neuron (2026), https://doi.org/10.1016/j.neuron.2026.03.031

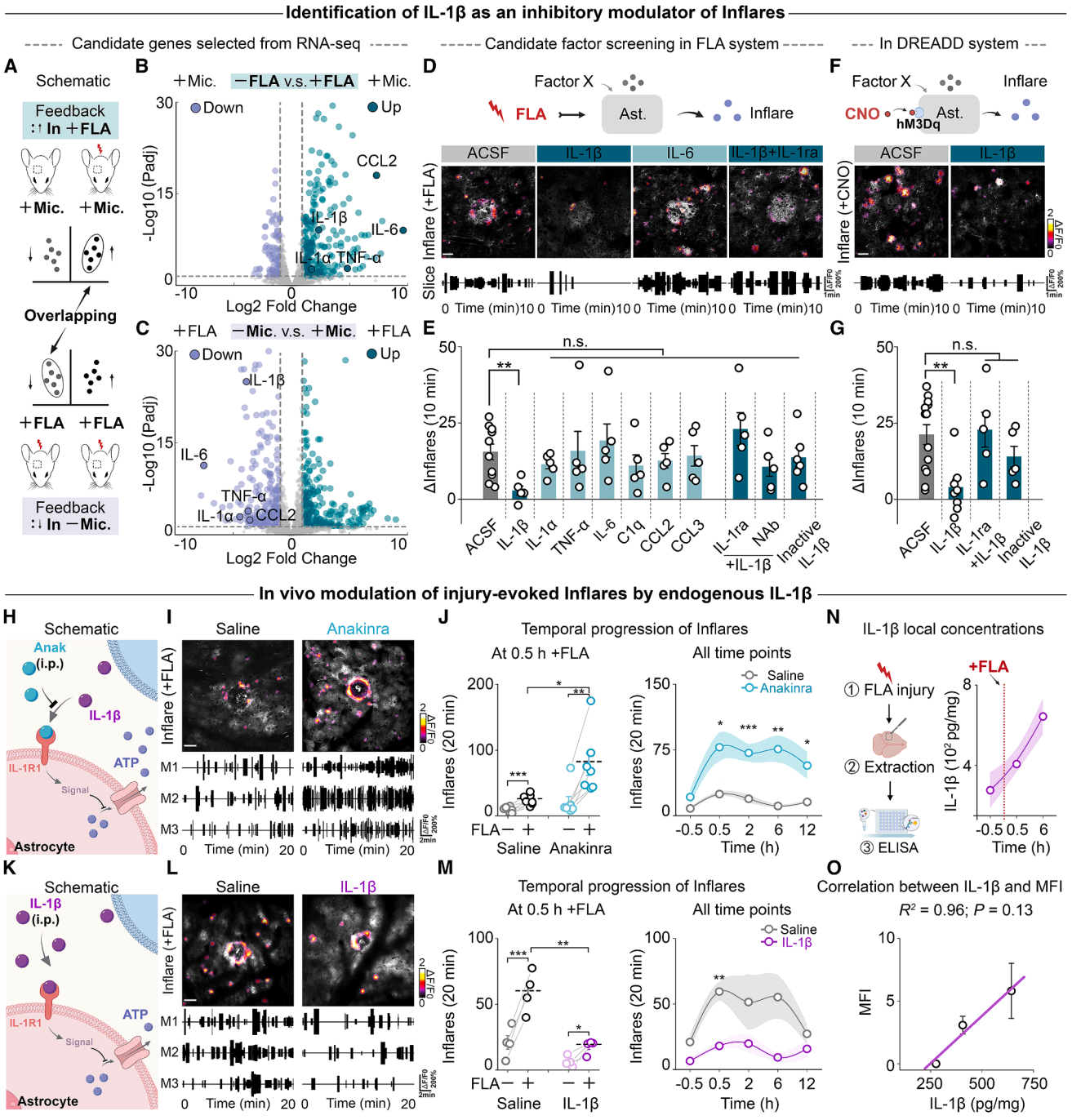

Figure 3. IL-1β acts as a primary inhibitory modulator of FLA-evoked Inflares

(A) Schematic illustrating the selection criteria for candidate mediators of microglial feedback on Inflares, which are upregulated following FLA (top) and downregulated upon microglia depletion (−Mic, bottom).

(B and C) Volcano plots showing differentially expressed genes between injured (+FLA) and uninjured (−FLA) tissues before and after FLA (B), and between injured tissues with or without microglia (C) (−FLA with microglia: $n = 3$ mice; +FLA with microglia: $n = 3$ mice; +FLA without microglia: $n = 5$ mice). Candidate genes meeting both criteria are labeled.

(D) Schematic (top), images (middle), and temporal distributions (bottom) of FLA-evoked Inflares in acute brain slices treated with the indicated factors.

(E) Group analysis of FLA-evoked changes in Inflare frequency (ΔInflare) across conditions (NAb, IL-1β neutralizing antibody) (artificial cerebrospinal fluid, ACSF: $n = 10$ slices/3 mice; IL-1β: $n = 5$ slices/3 mice; $p = 7.90 \times 10^{-3}$).

(F) Schematic (top), images (middle), and temporal distributions (bottom) of astrocytic hM_3Dq-evoked Inflares in acute brain slices treated with ACSF or IL-1β.

(G) Group analysis of astrocytic hM_3Dq-evoked changes in Inflares (ΔInflare) in each group (ACSF: $n = 13$ slices/5 mice; IL-1β: $n = 9$ slices/3 mice; $p = 1.40 \times 10^{-3}$).

(legend continued on next page)

Please cite this article in press as: Luan et al., A reciprocal glial circuit calibrates injury information and governs the tissue response balance, Neuron (2026), https://doi.org/10.1016/j.neuron.2026.03.031

transcriptomic analyses revealed that IL-1β is predominantly expressed by microglia with minor expression in a subset of astrocytes, whereas IL-1R1 is present in both cell types (Figures 4B–4D). This raises two possibilities: IL-1β may be released from microglia and act directly on astrocytic IL-1R1 (Figure 4A, top), or it may function indirectly via autocrine signaling on microglia (Figure 4A, bottom). To first test the ligand source, we generated transgenic mice harboring floxed *Il1b* alleles (*Il1b*-flox) and crossed them with a microglia-specific *Cx3cr1*-Cre recombinase fused with mutated estrogen receptor (CreERT) driver line (Figure 4E), enabling conditional deletion of *Il1b* in microglia with over 90% efficiency at the protein level and high cell-type specificity (Figures 4F, S8A, and S8B). In microglia-specific *Il1b* knockout mice (M-IL-1β-KO), equivalent FLA injuries elicited significantly elevated Inflare frequency and prolonged persistence of population Inflares over 12 h, compared with *Il1b*-flox littermates (Figures 4G and 4H; Video S4). By contrast, astrocyte-specific deletion of IL-1β effectively reduced IL-1β protein in astrocytes (Figures 4M and 4N) but did not produce detectable alteration in Inflares (Figures 4O and S7H–S7J), supporting that microglia are the dominant IL-1β source in the feedback circuit.

At the receptor level, the role of IL-1R1 was interrogated similarly by targeted gene deletions in a cell-type-specific manner (Figures 4I and 4J). Astrocyte-specific deletion of IL-1R1 acted as a phenocopy of microglial IL-1β deficiency, with similar sustained elevation of Inflares and reduced restitution over time after injury (Figures 4K and 4L; Video S5), strongly supporting the involvement of astrocytic IL-1R1 in directly sensing the inhibitory signal. Conversely, deleting IL-1R1 in microglia did not impact Inflare profiles (Figures 4P–4R and S7K–S7M), excluding autocrine signaling. Immunofluorescent staining confirmed the efficacy and cell-type specificity of the above manipulations (Figures S8C–S8H). Together, these results highlight the direct signaling axis in which microglial IL-1β directly stimulates astrocytic IL-1R for the feedback inhibition on Inflares.

Astrocytes integrate injury and microglial feedback through intracellular Ca^{2+}-calcineurin signaling

The above results position astrocytes as central integrators in the reciprocal glial circuit, simultaneously sensing both injury and microglial feedback to coordinate the generation of Inflares. Since injury promotes Inflares while IL-1β suppresses them, astrocytes must integrate these opposing cues intracellularly to produce a coherent output. We have previously demonstrated that astrocytic Ca^{2+} elevation is both necessary and sufficient for injury-evoked Inflares,[12] pointing to the possibility that Ca^{2+} and its related pathways may serve as intracellular integrators. Indeed, we observed that IL-1β effectively mobilizes astrocytic local Ca^{2+} transients with increased amplitude and spatial extent, which were reversed by the IL-1R1 antagonist (Figures 5A–5C). Removal of extracellular Ca^{2+} largely abolished the IL-1β-induced Ca^{2+} changes, whereas endoplasmic reticulum (ER) store depletion by thapsigargin was not effective (Figures 5D and S9A–S9F). Pharmacological screening further identified TRPV4 as the primary mediator of IL-1β-induced Ca^{2+} influx (Figures 5E, S9G, and S9H). By contrast, chemogenetic hM_3Dq-evoked Ca^{2+} events in astrocytes were predominantly dependent on intracellular Ca^{2+} stores and insensitive to the TRPV4 blocker (Figure S9I). Notably, we found that IL-1β-induced Ca^{2+} events are highly focal, in sharp contrast with the robust and propagative Ca^{2+} elevations elicited by chemogenetic activation (Figures S9J and S9K). These results suggest that distinct upstream mechanisms in astrocytes generate qualitatively different Ca^{2+} patterns that may differentially engage downstream events to control ATP release.

Among potential downstream effectors, the phosphatase calcineurin emerges as a compelling candidate due to its known role in coupling with IL-1R and regulating astrocytic activity and gene expression.[27] Indeed, the dephosphorylation of calcineurin substrate nuclear factor of activated T cells, cytoplasmic 3 (NFATc3) was detected in IL-1β-treated brain samples and was abolished by two independent calcineurin inhibitors (FK506 and CsA) (Figures S9L and S9M). To test whether calcineurin activity is required for the inhibitory effect of IL-1β, we pre-treated brain slices with calcineurin blockers, which effectively reversed the effect of IL-1β on Inflares in both injury- and astrocytic chemogenetically stimulated systems (Figures 5F–5H). Notably, only calcineurin inhibitors alone did not alter Inflare frequency, ruling out non-specific drug effects (Figures S10A–S10C).

To validate the mechanism *in vivo*, we genetically depleted the astrocytic calcineurin A-α (CNAα), the predominant catalytic subunit of calcineurin in astrocytes, using the CRISPR-Cas9 strategy (Figure 5I). Successful knockout of astrocytic CNAα was confirmed by immunohistochemistry in tissue, with a depletion efficiency over 50% (Figures 5J and S10D). Functionally, astrocytic CNAα-deficient mice exhibited substantially elevated Inflare frequency after injury (Figures 5K and 5L), indicating the loss of feedback inhibition. Importantly, inhibition of the downstream Panx1 hemichannel with probenecid (PBN) remained effective in suppressing Inflares, even under CNAα-deficient conditions (Figures 5M, S10E, and S10F), supporting the placement of Panx1 downstream of the Ca^{2+}-calcineurin axis. These data define astrocytic Ca^{2+}-calcineurin as a signal integration module

(H–J) Schematic (H), images and temporal distributions (I), and group analysis (J) of FLA-evoked Inflares *in vivo*, with the i.p. injection of saline or the IL-1β receptor antagonist Anakinra (10 mg/kg) (saline: $n = 8$ mice; $p = 2.10 \times 10^{-4}$; Anakinra: $n = 7$ mice; $p = 1.70 \times 10^{-3}$; $p = 2.36 \times 10^{-2}$, 4.30×10^{-4}, 7.70×10^{-3}, and 4.71×10^{-2} for 0.5, 2, 6, and 12 h, respectively).

(K–M) Similar to (H)–(J), except mice were injected with saline or IL-1β (10 μg/kg i.p.), and Inflares were recorded *in vivo* (saline: $n = 4$ mice; $p = 9.79 \times 10^{-4}$; IL-1β: $n = 4$ mice; $p = 3.17 \times 10^{-2}$; $p = 2.70 \times 10^{-3}$ for 0.5 between saline and IL-1β).

(N) Quantification of tissue IL-1β levels at indicated time points after FLA by ELISA ($n = 3$ mice).

(O) Correlation between IL-1β levels and microglial feedback index (MFI), matched across mice at equivalent time points ($n = 3$ mice for IL-1β and $n = 10$ mice for MFI).

Scale bars, 50 μm.

See Table S1 for statistics.

Please cite this article in press as: Luan et al., A reciprocal glial circuit calibrates injury information and governs the tissue response balance, Neuron (2026), https://doi.org/10.1016/j.neuron.2026.03.031

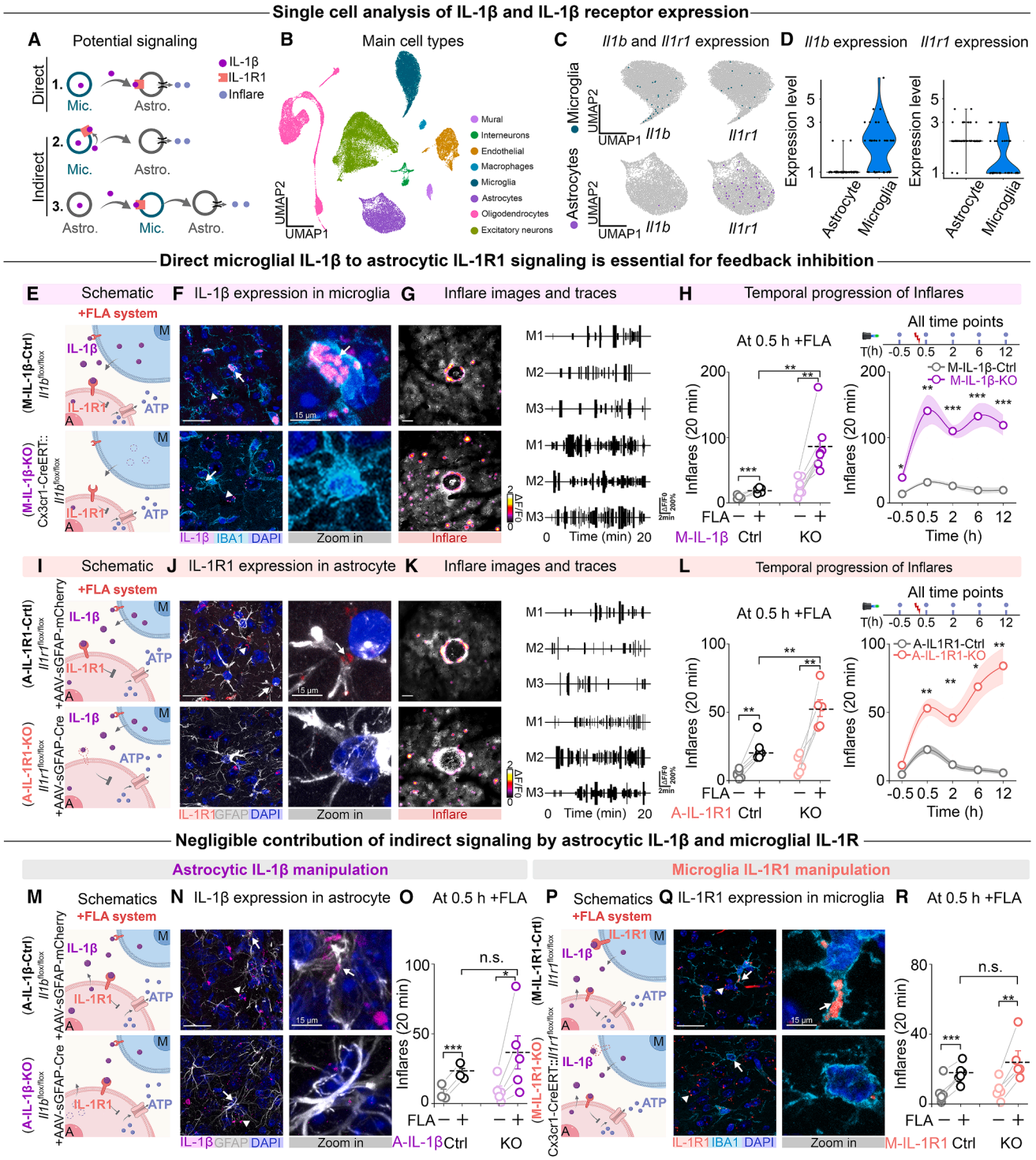

Figure 4. Direct IL-1β-IL-1R1 axis from microglia to astrocytes mediates feedback inhibition of Inflares

(A) Schematic illustrating potential cell-type-specific interactions between IL-1β and IL-1R1 in mediating feedback inhibition of Inflares.

(B–D) Clustering and annotation of single-cell RNA sequencing results and the expression profiles of *Il1b* and *Il1r1* in astrocytes and microglia.

(E–H) Schematic (E), immunofluorescence staining (F), images and temporal distributions (G), and group analysis (H) of FLA-evoked Inflares in *Il1b*-flox control mice (M-IL-1β-Ctrl, top) and microglia-specific IL-1β knockout mice (M-IL-1β-KO, bottom) ($n = 6$ mice in M-IL-1β-Ctrl; $n = 8$ mice in M-IL-1β-KO; $p = 2.50 \times 10^{-3}$ for +FLA between Ctrl and KO at 0.5 h). Arrows in (F) indicate IL-1β signals (magenta) in microglia (IBA1$^+$, cyan), while arrowheads mark IL-1β signals in other cell types (IBA1$^-$).

(legend continued on next page)

Please cite this article in press as: Luan et al., A reciprocal glial circuit calibrates injury information and governs the tissue response balance, Neuron (2026), https://doi.org/10.1016/j.neuron.2026.03.031

that decodes converging signals to regulate ATP output and ensure balanced injury responses *in vivo*.

Disbalance of the acute injury responses disrupts functional adaptations and compromises injury outcome

To explore how injury balance impacts outcomes, we first assessed microglial recruitment and morphology in astrocytic CNAα-deficient mice (A-CNAα-KO) and scrambled gRNA-expressing controls (Figure 6A). Deficiency of astrocytic calcineurin markedly enhanced microglial accumulation at the injury site (Figure 6B), consistent with the enhanced and prolonged Inflares. Moreover, microglial morphology showed exaggerated changes with enlarged soma and extended processes (Figure 6C), a potential primed activation state observed in disease models,[28] suggesting the multifaceted roles of microglia as both responders and regulators in the balanced injury response.

To further assess how injury dysregulation affects tissue function, we examined the adaptation of neural activities after injury. Thy1-GCaMP6f mice were used to record the visual stimulation-evoked Ca^{2+} activities in V1 cortical neurons before and after FLA injury in control and astrocytic calcineurin knockout mice (Figure 6D). In both groups, injury acutely silenced over 60% of neurons in the field-of-view (Figures 6E and 6F), mirroring the spatial spread of Inflares and suggesting a network-level disruption after injury.[29–31] Neuronal responsiveness exhibited partial recovery within 2 h after injury in control mice (Figure 6E), accompanied by increased inter-neuron synchrony, indicating the adaptive reorganization of local networks.[32] By contrast, astrocytic CNAα-KO mice failed to exhibit adaptive recovery of neural activities (Figures 6G, S11A, and S11B) and instead showed persistently impaired visual responses and reduced neuronal synchrony (Figures S11C and S11D). These mice also displayed elevated spontaneous Ca^{2+} activity in the absence of sensory stimuli (Figure S11E), which may reflect aberrant excitation or disinhibition that impairs sensory processing.

To further explore whether microglial IL-1β contributes to tissue-level outcomes through suppressing astrocytic ATP release, we established a traumatic brain injury model and assessed lesion size and cell apoptosis at both early and delayed time points using conditional deletion of microglial *Il1b* (Figure 6H). At 1-day post injury, loss of microglial IL-1β signaling resulted in a significant increase in lesion size at the tissue level, accompanied by elevated numbers of TUNEL-positive apoptotic cells in the peri-lesional region (Figures 6I and 6J). However, microglial deletion of *Il1b* produced injury outcomes comparable to those observed in control mice at 7 days post injury (Figures 6K and 6L), reflecting a temporally restricted contribution of microglial IL-1β to injury outcome. Collectively, these results suggest that glial interactions involving ATP and IL-1β signaling orchestrate multicellular adaptations that shape functional outcomes of acute brain injury.

DISCUSSION

Disruption of tissue balance is a hallmark and major driver of pathology.[33] As a result, most therapeutic strategies have focused on preventing the occurrence of injury or restoring the system back to physiological balance. Our findings reveal an active and internally regulated process that calibrates injury responses, emphasizing the importance of regulatory balance even under pathological conditions. Our work also identifies the reciprocal astrocyte-microglia feedback circuit and signaling mediators that govern the balance. These molecules may therefore provide targets for future diagnostic and therapeutic strategies in injury-related diseases.

Astrocytic Ca^{2+} signals were reported to be evoked by distinct mechanisms, exhibiting diverse patterns that differentially contribute to cellular functions.[34–36] In our case, the astrocytic Ca^{2+} signaling can both promote and suppress ATP Inflares. To explain this, we showed that chemogenetic activation induces robust and propagating Ca^{2+} waves that primarily depend on endoplasmic reticulum Ca^{2+} stores and functions to promote Inflare generation. Conversely, IL-1β-evoked Ca^{2+} signals are transient and spatially restricted, arising predominantly from Ca^{2+} influx, and suppress Inflares. These results provide a molecular basis for the divergent effects of astrocytic Ca^{2+} signaling on ATP Inflares.

While studies revealed the proinflammatory function of IL-1β and the beneficial effect of IL-1β blockade in injury or neurodegeneration,[37–39] our results support a complementary and previously underappreciated function of microglial IL-1β signaling, which acts as a negative feedback modulator on astrocytic ATP release during the acute phase of injury. Functionally, we showed that IL-1β, predominantly derived from microglia, act to restrain excessive activation of the initial injury response, whereas blockade of microglia-specific IL-1β signaling led to increased tissue damage and cell apoptosis at an early stage after traumatic brain injury. These findings indicate that the impact of IL-1β on injury outcome is both temporally controlled and cell-type dependent. In this regard, microglial IL-1β could represent an evolutionarily conserved mechanism to initially control the extent of damage upon focal injuries, which may

(I–L) Similar to (E)–(H), except experiments were performed in *Il1r1*-flox mice (A-IL-1R1-Ctrl, top) and astrocytic-specific IL-1R1 knockout mice (A-IL-1R1-KO, bottom) ($n = 6$ mice in A-IL-1R1-Ctrl; $n = 5$ mice in A-IL-1R1-KO; $p = 2.50 \times 10^{-3}$ for +FLA between Ctrl and KO at 0.5 h). Arrows in (J) indicate IL-1R1 signals (red) in astrocytes ($GFAP^+$, gray), while arrowheads indicate IL-1R1 in other cell types ($GFAP^-$).

(M–O) Schematic (M), immunofluorescence (N) and group analysis of FLA-evoked Inflares (O) in *Il1b*-flox (A-IL-1β-Ctrl, top) and astrocytic IL-1β knockout mice (A-IL-1β-KO) ($n = 3$ mice in A-IL-1β-Ctrl; $n = 5$ mice in A-IL-1β-KO; $p = 5.16 \times 10^{-4}$ for +FLA between −FLA and +FLA at Ctrl group, $p = 4.56 \times 10^{-2}$ for +FLA between −FLA and +FLA at KO group, $p = 0.45$ for +FLA between Ctrl and KO at 0.5 h).

(P–R) Similar to (M)–(O), except experiments were performed in *Il1r1*-flox mice (M-IL-1R1-Ctrl, top) and microglia-specific IL-1R1 knockout mice (M-IL-1R1-cKO, bottom) ($n = 6$ mice in M-IL-1R1-Ctrl; $n = 5$ mice in M-IL-1R1-KO; $p = 4.39 \times 10^{-4}$ for +FLA between −FLA and +FLA at the Ctrl group, $p = 7.00 \times 10^{-3}$ for +FLA between −FLA and +FLA at the KO group, $p = 0.18$ for +FLA between Ctrl and KO at 0.5 h).

Scale bars, 50 μm.

See Table S1 for statistics.

Please cite this article in press as: Luan et al., A reciprocal glial circuit calibrates injury information and governs the tissue response balance, Neuron (2026), https://doi.org/10.1016/j.neuron.2026.03.031

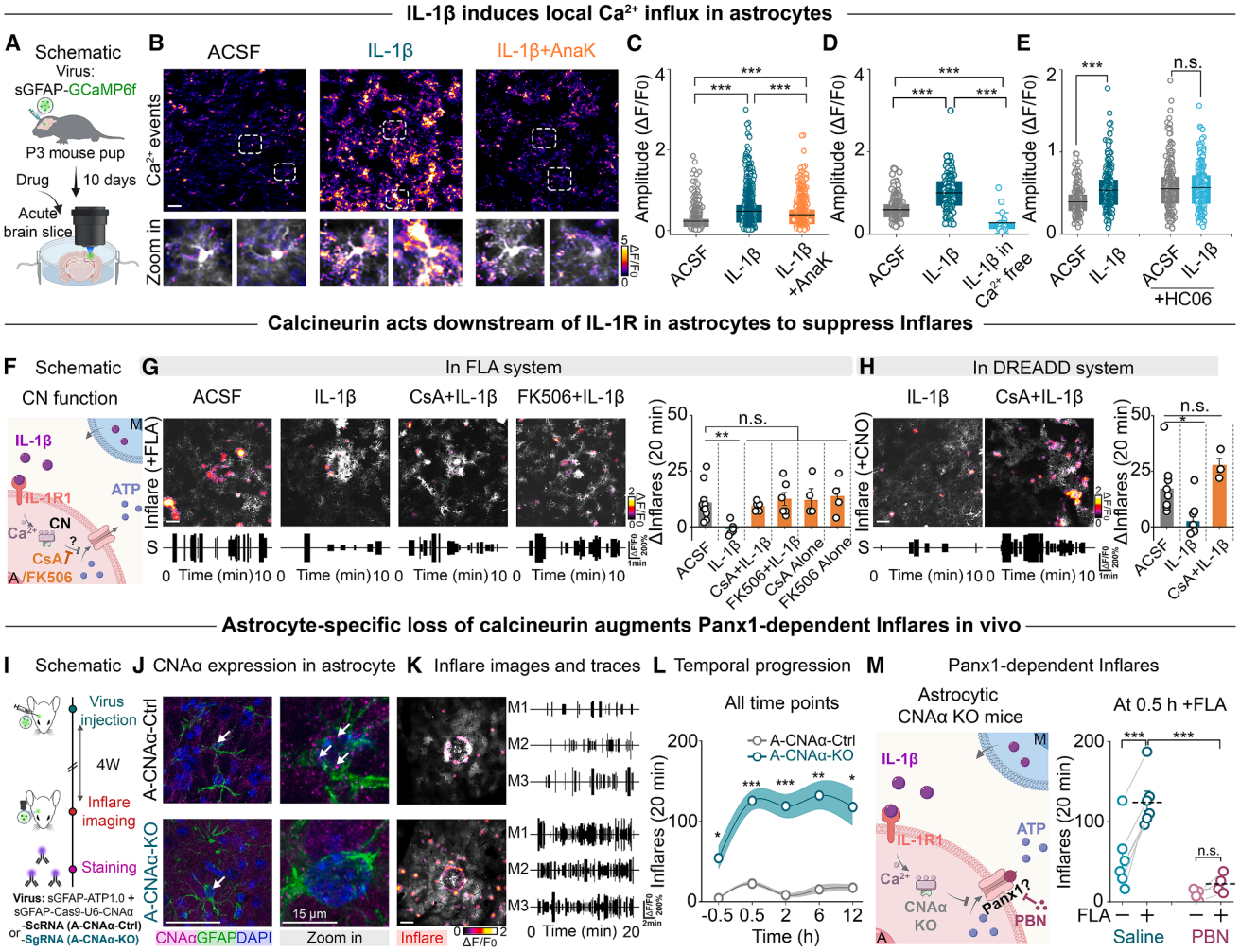

Figure 5. Astrocyte Ca^{2+}-calcineurin pathway integrates injury and microglial feedback signals to control pannexin-1-dependent Inflares

(A) Schematic of astrocytic Ca^{2+} imaging in acute brain slices subjected to different drug treatments.

(B) Representative images of astrocytic Ca^{2+} activity following ACSF, IL-1β, or IL-1β + Anakinra (AnaK) treatment.

(C) Group analysis of the amplitude of astrocytic Ca^{2+} signals across conditions (ACSF: n = 770 events/4 slices; IL-1β: n = 1426 events/6 slices; IL-1β+AnaK: n = 975 events/4 slices; Amplitude: $p = 1.28 \times 10^{-75}$ for ACSF and IL-1β; $p = 1.73 \times 10^{-7}$ for IL-1β and IL-1β+AnaK; $p = 1.31 \times 10^{-44}$ for ACSF and IL-1β+AnaK).

(D) Group analysis of the amplitude of astrocytic Ca^{2+} signals treated with ACSF, IL-1β, or IL-1β in Ca^{2+}-free buffer (ACSF: n = 251 events/3 slices; IL-1β: n = 184 events/3 slices; IL-1β in Ca^{2+} free: n = 22 events/4 slices; Amplitude: $p = 1.18 \times 10^{-24}$ for ACSF and IL-1β; $p = 1.92 \times 10^{-14}$ for IL-1β and IL-1β in Ca^{2+} free; $p = 9.26 \times 10^{-8}$ for ACSF and IL-1β in Ca^{2+} free).

(E) Group analysis of the IL-1β-evoked changes in astrocytic Ca^{2+} signals with or without HC06 (TRPV4 blocker) (ACSF: n = 324 events/3 slices; IL-1β: n = 322 events/3 slices; in HC06 group: ACSF: n = 381 events/5 slices; IL-1β+HC06: n = 326 events/5 slices; Amplitude: $p = 3.40 \times 10^{-15}$ for ACSF and IL-1β; $p = 0.23$ for ACSF and IL-1β+HC06).

(F and G) Schematic (F), images, temporal distributions and group analysis (G) of FLA-evoked Inflares in brain slices treated with indicated drugs (ACSF: n = 10 slices/3 mice; IL-1β: n = 6 slices/3 mice; CsA+IL-1β: n = 6 slices/3 mice; FK506+IL-1β: n = 6 slices/3 mice; CsA alone: n = 5 slices/3 mice; FK506 alone: n = 4 slices/3 mice; $p = 1.00 \times 10^{-3}$ for ACSF and IL-1β).

(H) Images, temporal distributions (left) and group analysis (right) of chemogenetically evoked Inflares in brain slices subjected to indicated drug treatments (ACSF: n = 9 slices/3 mice; IL-1β: n = 8 slices/3 mice; CsA+IL-1β: n = 3 slices/3 mice; $p = 1.30 \times 10^{-2}$ for ACSF and IL-1β).

(I–L) Schematic (I), immunofluorescence staining (J), images and temporal distributions (K), and group analysis (L) of FLA-evoked Inflares *in vivo* in mice expressing scrambled gRNA (A-CNAα-Ctrl, top) or CNAα-targeting sgRNA (A-CNAα-KO, bottom) (n = 6 mice; $p = 2.59 \times 10^{-2}$, 4.50×10^{-4}, 9.95×10^{-4}, 1.20×10^{-3}, and 1.11×10^{-2} for −0.5, 0.5, 2, 6, and 12 h, respectively).

(M) Schematic and group analysis of FLA-evoked Inflares in astrocytic calcineurin knockout mice (A-CNAα-KO) treated with saline or the pannexin-1 blocker probenecid (PBN, 200 mg/kg) (n = 6 mice in saline; n = 4 mice in PBN; $p = 3.56 \times 10^{-4}$ for +FLA between saline and PBN).

Scale bars, 50 μm. All statistical tests were two-sided.

See Table S1 for statistics.

Please cite this article in press as: Luan et al., A reciprocal glial circuit calibrates injury information and governs the tissue response balance, Neuron (2026), https://doi.org/10.1016/j.neuron.2026.03.031

CellPress

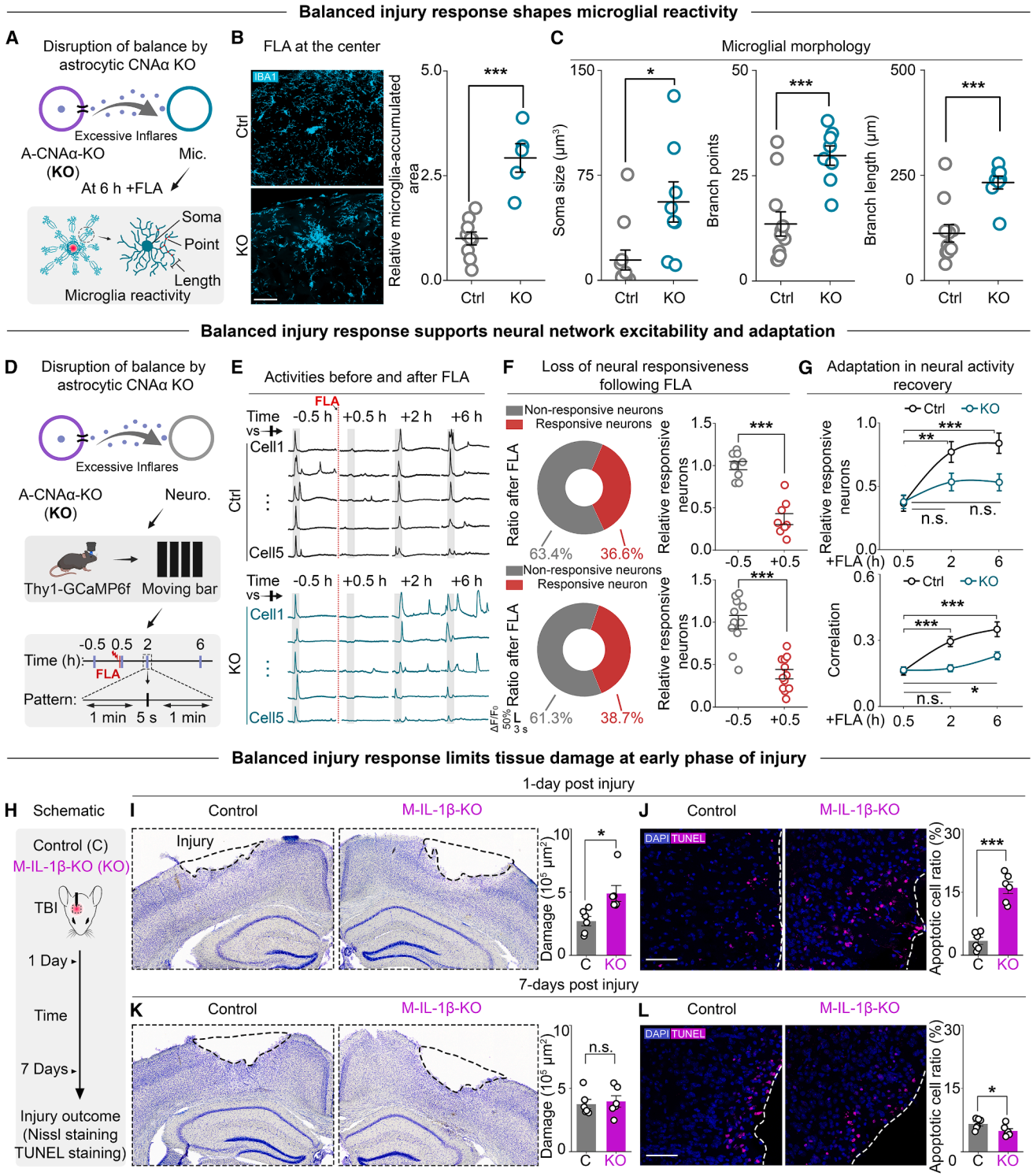

Figure 6. Disruption of balanced injury response impairs cellular reactivity and exacerbates early-phase injury outcomes

(A) Schematic showing the disruption of balanced injury response in astrocytic CNAα knockout mice (top) and the consequence on microglia (bottom).

(B) Representative images and quantification of microglia accumulation at the injury center at 6 h after FLA in scrambled-gRNA control (Ctrl) or astrocytic CNAα knockout mice (KO) (Ctrl: $n = 9$ regions from 3 mice; KO: $n = 5$ regions from 3 mice; $p = 6.80 \times 10^{-5}$). Microglia accumulation was quantified by measuring the microglial area at the injury center and normalizing it to the average value in the Ctrl group.

(legend continued on next page)

be overridden by different processes, including the extent of tissue injury, changes of blood-brain barrier (BBB) integrity, and systemic inflammation, making the functions of IL-1β largely context-dependent in different disease states. Thus, future studies should aim to precisely map the contribution of IL-1β and its regulatory mechanisms in order to identify the most optimal targeting strategies that limit detrimental outcomes while preserving beneficial effects. A similar logic may also apply to astrocytic calcineurin, whose canonical proinflammatory effect and the newly revealed inhibitory control of ATP release can be viewed as the context-dependent reprogramming across states.[27,40]

Altogether, our findings support a revised view of injury pathology, in which outcomes are shaped not only by damage itself but also by the internal organization or disruption of glial feedback circuits. The molecular dialogue highlights the ability of glia to actively process injury-related signals, opening new directions for exploring their broader roles in disease and their rational targeting in therapeutics.

Limitations of the study

The glial circuit described here was primarily characterized in the visual cortex of adult mice using acute injury models. Given the heterogeneity of astrocyte and microglia responses across brain regions, developmental stages, and injury types,[41,42] whether this mechanism generalizes to other contexts remains to be investigated. Further work will also be required to determine how distinct astrocytic Ca^{2+} dynamics are translated into differential ATP release outcomes.

RESOURCE AVAILABILITY

Lead contact

Requests for further information and resources should be directed to and will be fulfilled by the lead contact, Miao Jing (jingmiao@cibr.ac.cn).

Materials availability

This study did not generate any new, unique reagents.

Data and code availability

- Data availability: all data reported in this paper will be shared by the lead contact upon request. The source data statistical analysis is available in Table S1 of the manuscript. All the sequencing data have been deposited in the NCBI Sequence Read Archive (SRA): https://www.ncbi.nlm.nih.gov/sra/PRJNA1396901, and the single-cell RNA sequencing analysis was performed using a publicly available dataset from the NCBI GEO under accession number GEO: GSE102827. Microscopy data and original western blot images reported in this paper will be shared by the lead contact upon request.
- Code: all original codes used in the study are available on GitHub: https://github.com/JingMiaoLab/NEURON-D-25-01766 and archived at Zenodo: 10.5281/zenodo.19107777.
- Any additional information required to reanalyze the data reported in this paper is available from the lead contact upon request.

ACKNOWLEDGMENTS

We thank Minmin Luo, Hu Zhao, and Jingfeng Zhou at the Chinese Institute for Brain Research (CIBR); Min Xu and Zhaofa Wu at the Chinese Academy of Science for sharing transgenic mice; Wei Shi at CIBR for sharing antibodies; the core facilities at CIBR for assistance with optical imaging, mice, and the AAV package; and the cell biology/light microscopy core facilities at HUN-REN KOKI for experimental assistance. Some schematics were created using BioRender. This work was supported by the STI2030-Major project 2021ZD0202200, subject 2021ZD0202203 (M.J.); the Project of Intergovernmental Science and Technology Innovative Cooperation, National Key Research and Development program 2021YFE0116400 (M.J.); the CAMS Innovation Fund for Medical Sciences (CIFMS) 2024-I2M-3-023 (M.J.); the applied research and development projects in Hungarian-Chinese cooperation 2020-1.2.4-TÉT-IPARI-2021-00005 (Á.D.); the "Momentum" research grant from the Hungarian Academy of Sciences LP2022-5/2022 to (Á.D.); the Hungarian Brain Research Program (grant no. NAP2022-I-1/2022 to Á.D.); and the National Research, Development, and Innovation Fund, the DP-2021 funding scheme KDP-12-10/PALY-2022 (A.D.S.).

AUTHOR CONTRIBUTIONS

P.L. performed experiments related to *in vitro* and *in vivo* imaging and mechanistic studies with the help of X.J.; J.J. performed brain slice-related experiments and immunofluorescence; Y.C. contributed to data analysis related to Inflare signals and neural activities; F.X. performed molecular and biochemical experiments with the help of Y.W.; A.D.S. performed chemogenetic microglia manipulation, *in vivo* two-photon imaging, and histology under the supervision of Á.D.; Z.K. and B.K. performed ATP detection in cultured astrocytes; M.J. conceived the study with input from Á.D. on experiment design and overall concept; P.L., Á.D., and M.J. wrote and edited the manuscript with input from all authors; and M.J. and Á.D. obtained funding and provided resources for the project.

(C) Group analysis of microglial morphology in Ctrl and KO mice at 6 h after FLA, including soma size (left, Ctrl: $n = 11$ cells from 3 mice; KO: $n = 8$ cells from 3 mice; $p = 1.19 \times 10^{-2}$), branch points (middle, Ctrl: $n = 11$ cells from 3 mice; KO: $n = 8$ cells from 3 mice; $p = 6.65 \times 10^{-4}$), and branch length (right, Ctrl: $n = 11$ cells from 3 mice; KO: $n = 8$ cells from 3 mice; $p = 4.32 \times 10^{-4}$).
(D) Schematic showing the disruption of balanced injury response and the consequence on visual-stimulation-evoked neural activity in Thy1-GCaMP6 mice.
(E) Representative traces showing the neural Ca^{2+} activities at baseline and indicated time points after FLA (right), in both control (Ctrl) and astrocytic CNAα knockout (KO) mice. Dashed regions indicate periods of visual stimulation.
(F) Quantification of the proportion of neurons that lost visual-evoked responses at 0.5 h after FLA (Ctrl: $n = 9$ trials from 3 mice; KO: $n = 12$ trials from 4 mice; $p = 8.54 \times 10^{-7}$ for Ctrl; $p = 2.24 \times 10^{-6}$ for KO).
(G) Top, time course showing the recovery of visual responsive neurons after FLA in Ctrl and astrocytic-CNAα KO mice (Ctrl: $n = 9$ trials from 3 mice; $p = 1.80 \times 10^{-3}$, $p = 4.30 \times 10^{-4}$ for 2 and 6 h compared with 0.5 h; KO: $n = 12$ trials from 4 mice; $p = 0.10$, $p = 9.87 \times 10^{-2}$ for 2 and 6 h compared with 0.5 h). Bottom, average correlation of visual-evoked neural activity at different time points after FLA (Ctrl: $n = 9$ trials from 3 mice; $p = 5.43 \times 10^{-4}$, $p = 2.57 \times 10^{-4}$ for 2 and 6 h compared with 0.5 h; KO: $n = 12$ trials from 4 mice; $p = 0.70$, $p = 1.09 \times 10^{-2}$ for 2 and 6 h compared with 0.5 h).
(H) The procedure to assess injury outcomes at different phases following traumatic brain injury (TBI) in WT and microglial-*Il1b*-knockout mice.
(I) Representative Nissl staining and quantification of lesion area at 1-day post injury in WT and microglial-*Il1b*-knockout mice ($n = 6$ mice; $p = 1.39 \times 10^{-2}$).
(J) Representative TUNEL staining and quantification of apoptotic cells in WT and microglial-*Il1b*-knockout mice ($n = 6$ mice; $p = 1.42 \times 10^{-5}$)
(K and L) Similar to (I) and (J), except the assays were performed at 7 days post injury ($n = 6$ mice; $p = 0.73$ in damage; $p = 0.049$ in apoptotic cell ratio).
Scale bars, 50 μm.
See Table S1 for statistics.

DECLARATION OF INTERESTS

The authors declare no competing interests.

STAR★METHODS

Detailed methods are provided in the online version of this paper and include the following:

- KEY RESOURCES TABLE
- EXPERIMENTAL MODEL AND STUDY PARTICIPANT DETAILS
  - Animals
  - Viruses
- METHOD DETAILS
  - Stereotaxic surgery and virus injection
  - Acute brain slice preparation
  - Microglia depletion and repopulation
  - Two-photon imaging and focal laser ablation (FLA)
  - Traumatic brain injury
  - Measurement of ATP levels in cell cultures
  - Drug administration
  - Secreted IL-1β protein detection
  - Cell apoptosis detection
  - Nissl staining
  - Immunofluorescence staining and Western blot
  - Gene expression profiling
  - Visual stimulation
  - Data analysis
- QUANTIFICATION AND STATISTICAL ANALYSIS

SUPPLEMENTAL INFORMATION

Supplemental information can be found online at https://doi.org/10.1016/j.neuron.2026.03.031.

Received: August 14, 2025
Revised: February 4, 2026
Accepted: March 20, 2026

REFERENCES

1. GBD 2016 Traumatic Brain Injury and Spinal Cord Injury Collaborators (2019). Global, Regional, and National Burden of Traumatic Brain Injury and Spinal Cord Injury, 1990–2016: A Systematic Analysis for the Global Burden of Disease Study 2016. Lancet Neurol. (James Publishing) *18*, 56–87. https://doi.org/10.1016/S1474-4422(18)30415-0.
2. Simon, D.W., McGeachy, M.J., Bayır, H., Clark, R.S., Loane, D.J., and Kochanek, P.M. (2017). The far-reaching scope of neuroinflammation after traumatic brain injury. Nat. Rev. Neurol. *13*, 171–191. https://doi.org/10.1038/nrneurol.2017.13.
3. Rolls, A., Shechter, R., and Schwartz, M. (2009). The bright side of the glial scar in CNS repair. Nat. Rev. Neurosci. *10*, 235–241. https://doi.org/10.1038/nrn2591.
4. Burda, J.E., Bernstein, A.M., and Sofroniew, M.V. (2016). Astrocyte roles in traumatic brain injury. Exp. Neurol. *275*, 305–315. https://doi.org/10.1016/j.expneurol.2015.03.020.
5. Loane, D.J., and Kumar, A. (2016). Microglia in the TBI brain: The good, the bad, and the dysregulated. Exp. Neurol. *275*, 316–327. https://doi.org/10.1016/j.expneurol.2015.08.018.
6. Bezzi, P., Domercq, M., Brambilla, L., Galli, R., Schols, D., De Clercq, E., Vescovi, A., Bagetta, G., Kollias, G., Meldolesi, J., and Volterra, A. (2001). CXCR4-activated astrocyte glutamate release via TNFalpha: amplification by microglia triggers neurotoxicity. Nat. Neurosci. *4*, 702–710. https://doi.org/10.1038/89490.
7. Colombo, E., and Farina, C. (2016). Astrocytes: Key Regulators of Neuroinflammation. Trends Immunol. *37*, 608–620. https://doi.org/10.1016/j.it.2016.06.006.
8. Vainchtein, I.D., Chin, G., Cho, F.S., Kelley, K.W., Miller, J.G., Chien, E.C., Liddelow, S.A., Nguyen, P.T., Nakao-Inoue, H., Dorman, L.C., et al. (2018). Astrocyte-derived interleukin-33 promotes microglial synapse engulfment and neural circuit development. Science *359*, 1269–1273. https://doi.org/10.1126/science.aal3589.
9. Davalos, D., Grutzendler, J., Yang, G., Kim, J.V., Zuo, Y., Jung, S., Littman, D.R., Dustin, M.L., and Gan, W.B. (2005). ATP mediates rapid microglial response to local brain injury in vivo. Nat. Neurosci. *8*, 752–758. https://doi.org/10.1038/nn1472.
10. Haynes, S.E., Hollopeter, G., Yang, G., Kurpius, D., Dailey, M.E., Gan, W.B., and Julius, D. (2006). The P2Y12 receptor regulates microglial activation by extracellular nucleotides. Nat. Neurosci. *9*, 1512–1519. https://doi.org/10.1038/nn1805.
11. Cauwels, A., Rogge, E., Vandendriessche, B., Shiva, S., and Brouckaert, P. (2014). Extracellular ATP drives systemic inflammation, tissue damage and mortality. Cell Death Dis. *5*, e1102. https://doi.org/10.1038/cddis.2014.70.
12. Chen, Y., Luan, P., Liu, J., Wei, Y., Wang, C., Wu, R., Wu, Z., and Jing, M. (2024). Spatiotemporally selective astrocytic ATP dynamics encode injury information sensed by microglia following brain injury in mice. Nat. Neurosci. *27*, 1522–1533. https://doi.org/10.1038/s41593-024-01680-w.
13. Marker, D.F., Tremblay, M.E., Lu, S.M., Majewska, A.K., and Gelbard, H.A. (2010). A thin-skull window technique for chronic two-photon in vivo imaging of murine microglia in models of neuroinflammation. J. Vis. Exp. *43*, e2059. https://doi.org/10.3791/2059.
14. Zajicek, G. (1999). Wisdom of the body. Med. Hypotheses *52*, 447–449. https://doi.org/10.1054/mehy.1997.0679.
15. Matejuk, A., and Ransohoff, R.M. (2020). Crosstalk Between Astrocytes and Microglia: An Overview. Front. Immunol. *11*, 1416. https://doi.org/10.3389/fimmu.2020.01416.
16. Antonioli, L., Pacher, P., Vizi, E.S., and Haskó, G. (2013). CD39 and CD73 in immunity and inflammation. Trends Mol. Med. *19*, 355–367. https://doi.org/10.1016/j.molmed.2013.03.005.
17. Paolicelli, R.C., Sierra, A., Stevens, B., Tremblay, M.E., Aguzzi, A., Ajami, B., Amit, I., Audinat, E., Bechmann, I., Bennett, M., et al. (2022). Microglia states and nomenclature: A field at its crossroads. Neuron *110*, 3458–3483. https://doi.org/10.1016/j.neuron.2022.10.020.
18. Hammond, T.R., Dufort, C., Dissing-Olesen, L., Giera, S., Young, A., Wysoker, A., Walker, A.J., Gergits, F., Segel, M., Nemesh, J., et al. (2019). Single-Cell RNA Sequencing of Microglia throughout the Mouse Lifespan and in the Injured Brain Reveals Complex Cell-State Changes. Immunity *50*, 253–271. https://doi.org/10.1016/j.immuni.2018.11.004.
19. Jia, J., Zheng, L., Ye, L., Chen, J., Shu, S., Xu, S., Bao, X., Xia, S., Liu, R., Xu, Y., et al. (2023). CD11c+ microglia promote white matter repair after ischemic stroke. Cell Death Dis. *14*, 156. https://doi.org/10.1038/s41419-023-05689-0.
20. Keren-Shaul, H., Spinrad, A., Weiner, A., Matcovitch-Natan, O., Dvir-Szternfeld, R., Ulland, T.K., David, E., Baruch, K., Lara-Astaiso, D., Toth, B., et al. (2017). A Unique Microglia Type Associated with Restricting Development of Alzheimer's Disease. Cell *169*, 1276–1290. https://doi.org/10.1016/j.cell.2017.05.018.
21. Yu, T., Zhang, X., Shi, H., Tian, J., Sun, L., Hu, X., Cui, W., and Du, D. (2019). P2Y12 regulates microglia activation and excitatory synaptic transmission in spinal lamina II neurons during neuropathic pain in rodents. Cell Death Dis. *10*, 165. https://doi.org/10.1038/s41419-019-1425-4.
22. Császár, E., Lénárt, N., Cserép, C., Környei, Z., Fekete, R., Pósfai, B., Balázsfi, D., Hangya, B., Schwarcz, A.D., Szabadits, E., et al. (2022). Microglia modulate blood flow, neurovascular coupling, and hypoperfusion via purinergic actions. J. Exp. Med. *219*, e20211071. https://doi.org/10.1084/jem.20211071.

23. Klawonn, A.M., Fritz, M., Castany, S., Pignatelli, M., Canal, C., Similä, F., Tejeda, H.A., Levinsson, J., Jaarola, M., Jakobsson, J., et al. (2021). Microglial activation elicits a negative affective state through prostaglandin-mediated modulation of striatal neurons. Immunity *54*, 225–234. https://doi.org/10.1016/j.immuni.2020.12.016.

24. Nakamura, Y. (2002). Regulating factors for microglial activation. Biol. Pharm. Bull. *25*, 945–953. https://doi.org/10.1248/bpb.25.945.

25. Chen, M., Li, Y., Huang, J., Wang, Y., and Zhao, H. (2025). Generation of the Ci1 Reporter Mouse Strain with Enhanced Fluorescence for Tissue Clearing Applications. Neurosci. Bull. *41*, 1317–1328. https://doi.org/10.1007/s12264-025-01421-4.

26. Bresnihan, B., Alvaro-Gracia, J.M., Cobby, M., Doherty, M., Domljan, Z., Emery, P., Nuki, G., Pavelka, K., Rau, R., Rozman, B., et al. (1998). Treatment of rheumatoid arthritis with recombinant human interleukin-1 receptor antagonist. Arthritis Rheum. *41*, 2196–2204. https://doi.org/10.1002/1529-0131(199812)41:12<2196::AID-ART15>3.0.CO;2-2.

27. Lim, D., Tapella, L., Dematteis, G., Talmon, M., and Genazzani, A.A. (2023). Calcineurin Signalling in Astrocytes: From Pathology to Physiology and Control of Neuronal Functions. Neurochem. Res. *48*, 1077–1090. https://doi.org/10.1007/s11064-022-03744-4.

28. Perry, V.H., and Holmes, C. (2014). Microglial priming in neurodegenerative disease. Nat. Rev. Neurol. *10*, 217–224. https://doi.org/10.1038/nrneurol.2014.38.

29. Frankowski, J.C., Foik, A.T., Tierno, A., Machhor, J.R., Lyon, D.C., and Hunt, R.F. (2021). Traumatic brain injury to primary visual cortex produces long-lasting circuit dysfunction. Commun. Biol. *4*, 1297. https://doi.org/10.1038/s42003-021-02808-5.

30. Eysel, U.T., and Schweigart, G. (1999). Increased receptive field size in the surround of chronic lesions in the adult cat visual cortex. Cereb. Cortex *9*, 101–109. https://doi.org/10.1093/cercor/9.2.101.

31. Imbrosci, B., Eysel, U.T., and Mittmann, T. (2010). Metaplasticity of horizontal connections in the vicinity of focal laser lesions in rat visual cortex. J. Physiol. *588*, 4695–4703. https://doi.org/10.1113/jphysiol.2010.198192.

32. Ding, M.C., Wang, Q., Lo, E.H., and Stanley, G.B. (2011). Cortical excitation and inhibition following focal traumatic brain injury. J. Neurosci. *31*, 14085–14094. https://doi.org/10.1523/JNEUROSCI.3572-11.2011.

33. Cannon, W.B. (1929). Organization for physiological homeostasis. Physiol. Rev. *9*, 399–431. https://doi.org/10.1152/physrev.1929.9.3.399.

34. Kol, A., Adamsky, A., Groysman, M., Kreisel, T., London, M., and Goshen, I. (2020). Astrocytes contribute to remote memory formation by modulating hippocampal-cortical communication during learning. Nat. Neurosci. *23*, 1229–1239. https://doi.org/10.1038/s41593-020-0679-6.

35. Benoit, L., Hristovska, I., Liaudet, N., Jouneau, P.H., Fertin, A., de Ceglia, R., Litvin, D.G., Di Castro, M.A., Jevtic, M., Zalachoras, I., et al. (2025). Astrocytes functionally integrate multiple synapses via specialized leaflet domains. Cell *188*, 6453–6472. https://doi.org/10.1016/j.cell.2025.08.036.

36. Srinivasan, R., Huang, B.S., Venugopal, S., Johnston, A.D., Chai, H., Zeng, H., Golshani, P., and Khakh, B.S. (2015). Ca(2+) signaling in astrocytes from Ip3r2(-/-) mice in brain slices and during startle responses in vivo. Nat. Neurosci. *18*, 708–717. https://doi.org/10.1038/nn.4001.

37. Allan, S.M., and Rothwell, N.J. (2001). Cytokines and acute neurodegeneration. Nat. Rev. Neurosci. *2*, 734–744. https://doi.org/10.1038/35094583.

38. Allan, S.M., Tyrrell, P.J., and Rothwell, N.J. (2005). Interleukin-1 and neuronal injury. Nat. Rev. Immunol. *5*, 629–640. https://doi.org/10.1038/nri1664.

39. Heneka, M.T., Kummer, M.P., and Latz, E. (2014). Innate immune activation in neurodegenerative disease. Nat. Rev. Immunol. *14*, 463–477. https://doi.org/10.1038/nri3705.

40. Tapella, L., Dematteis, G., Ruffinatti, F.A., Ponzoni, L., Fiordaliso, F., Corbelli, A., Albanese, E., Pistolato, B., Pagano, J., Barberis, E., et al. (2021). Deletion of calcineurin from astrocytes reproduces proteome signature of Alzheimer's disease and epilepsy and predisposes to seizures. Cell Calcium *100*, 102480. https://doi.org/10.1016/j.ceca.2021.102480.

41. Khakh, B.S., and Deneen, B. (2019). The Emerging Nature of Astrocyte Diversity. Annu. Rev. Neurosci. *42*, 187–207. https://doi.org/10.1146/annurev-neuro-070918-050443.

42. Fumagalli, L., Nazlie Mohebiany, A., Premereur, J., Polanco Miquel, P., Bijnens, B., Van de Walle, P., Fattorelli, N., and Mancuso, R. (2025). Microglia heterogeneity, modeling and cell-state annotation in development and neurodegeneration. Nat. Neurosci. *28*, 1381–1392. https://doi.org/10.1038/s41593-025-01931-4.

43. Wang, Y., DelRosso, N.V., Vaidyanathan, T.V., Cahill, M.K., Reitman, M.E., Pittolo, S., Mi, X., Yu, G., and Poskanzer, K.E. (2019). Accurate quantification of astrocyte and neurotransmitter fluorescence dynamics for single-cell and population-level physiology. Nat. Neurosci. *22*, 1936–1944. https://doi.org/10.1038/s41593-019-0492-2.

44. Yang, G., Pan, F., Parkhurst, C.N., Grutzendler, J., and Gan, W.B. (2010). Thinned-skull cranial window technique for long-term imaging of the cortex in live mice. Nat. Protoc. *5*, 201–208. https://doi.org/10.1038/nprot.2009.222.

45. Wu, Z., He, K., Chen, Y., Li, H., Pan, S., Li, B., Liu, T., Xi, F., Deng, F., Wang, H., et al. (2022). A sensitive GRAB sensor for detecting extracellular ATP in vitro and in vivo. Neuron *110*, 770–782. https://doi.org/10.1016/j.neuron.2021.11.027.

46. Xiong, Y., Mahmood, A., and Chopp, M. (2013). Animal models of traumatic brain injury. Nat. Rev. Neurosci. *14*, 128–142. https://doi.org/10.1038/nrn3407.

47. Glushakova, O.Y., Glushakov, A.O., Borlongan, C.V., Valadka, A.B., Hayes, R.L., and Glushakov, A.V. (2018). Role of Caspase-3-Mediated Apoptosis in Chronic Caspase-3-Cleaved Tau Accumulation and Blood-Brain Barrier Damage in the Corpus Callosum after Traumatic Brain Injury in Rats. J. Neurotrauma *35*, 157–173. https://doi.org/10.1089/neu.2017.4999.

48. Környei, Z., Szlávik, V., Szabó, B., Gócza, E., Czirók, A., and Madarász, E. (2005). Humoral and contact interactions in astroglia/stem cell co-cultures in the course of glia-induced neurogenesis. Glia *49*, 430–444. https://doi.org/10.1002/glia.20123.

49. Chen, T.W., Wardill, T.J., Sun, Y., Pulver, S.R., Renninger, S.L., Baohan, A., Schreiter, E.R., Kerr, R.A., Orger, M.B., Jayaraman, V., et al. (2013). Ultrasensitive fluorescent proteins for imaging neuronal activity. Nature *499*, 295–300. https://doi.org/10.1038/nature12354.

Please cite this article in press as: Luan et al., A reciprocal glial circuit calibrates injury information and governs the tissue response balance, Neuron (2026), https://doi.org/10.1016/j.neuron.2026.03.031

STAR★METHODS

KEY RESOURCES TABLE

REAGENT or RESOURCE	SOURCE	IDENTIFIER
Antibodies		
Rabbit monoclonal anti-Iba1	Abcam	Cat# ab178846; RRID: AB_2636859
Mouse monoclonal anti-Iba1	Abcam	Cat# ab283319; RRID: AB_2924797
Goat monoclonal anti-Iba1	Abcam	Cat# ab289874; RRID: AB_2942069
Chicken polyclonal anti-GFAP	Abcam	Cat# ab4674; RRID: AB_304558
Rabbit monoclonal anti-NeuN	Abcam	Cat# ab177487; RRID: AB_2532109
Mouse monoclonal anti-NeuN	Abcam	Cat# ab104224; RRID: AB_10711040
Rat monoclonal anti-NeuN	Abcam	Cat# ab279297; RRID: AB_3095692
Rabbit monoclonal anti-P2Y12	Abcam	Cat# ab300140; RRID: AB_3677650
Rabbit monoclonal anti-HA tag	Abcam	Cat# ab236632; RRID: AB_2864361
Rabbit monoclonal anti-IL-1β	Abcam	Cat# ab254360; RRID: AB_2936299
Mouse polyclonal anti-IL-1R1	Invitrogen	Cat# PA547937; RRID: AB_2609445
Rabbit monoclonal anti-Calcineurin A	Abcam	Cat# ab109412; RRID: AB_10858173
Mouse monoclonal anti- p-NFATc3	Santa Cruz Biotechnology	Cat# sc-365786; RRID: AB_10844623
Rabbit monoclonal anti-GAPDH	Cell signaling technology	Cat# 2118S; RRID: AB_561053
Chicken Polyclonal anti-eGFP	Thermo Fisher Scientific	Cat# A10262; RRID: AB_2534023
Guinea pig Polyclonal anti-CD11c	Synaptic Systems	Cat# HS-375 004; RRID: AB_2800541
Donkey Anti-Guinea pig IgG H&L (Alexa Fluor 647)	Jackson ImmunoResearch Labs	Cat# 706-606-148; RRID: AB_2340477
Donkey Anti-Chicken IgG H&L (Alexa Fluor 488)	Jackson ImmunoResearch Labs	Cat# 703-546-155; RRID: AB_2340376
Donkey Anti-Goat IgG H&L (Alexa Fluor 488)	Jackson ImmunoResearch Labs	Cat# 705-545-147; RRID: AB_2336933
Donkey Anti-Goat IgG H&L (Alexa Fluor 647)	Invitrogen	Cat# A21447; RRID: AB_141844
Donkey Anti-Goat IgG H&L (Alexa Fluor 488)	Abcam	Cat# ab150129; RRID: AB_2687506
Cy3-AffiniPure Donkey Anti-Rabbit IgG (H+L)	Jackson ImmunoResearch Labs	Cat# 711-165-152; RRID: AB_2307443
Donkey Anti-Mouse IgG H&L (Alexa Fluor 488)	Jackson ImmunoResearch Labs	Cat# 715-545-151; RRID: AB_2341099
Alexa Fluor 594-AffiniPure Donkey Anti-Mouse IgG (H+L)	Jackson ImmunoResearch Labs	Cat# 715-585-150; RRID: AB_2340854
Alexa Fluor 647-AffiniPure Donkey Anti-Rabbit IgG (H+L)	Jackson ImmunoResearch Labs	Cat# 711-605-152; RRID: AB_2492288
Goat Anti-Mouse IgG H&L (Alexa Fluor 555)	Abcam	Cat# ab150114; RRID: AB_2687594
Goat Anti-Chicken IgY H&L (Alexa Fluor® 647)	Abcam	Cat# ab150171; AB_2800541: AB_2921318
Goat Anti-Mouse IgG H&L (Alexa Fluor® 488)	Abcam	Cat# ab150113; RRID: AB_2576208
HRP-conjugated Rabbit anti-mouse IgG H&L	Abcam	Cat# ab6728; RRID: AB_955440
Goat Anti-Rabbit IgG H&L (HRP)	Abcam	Cat# ab6721; RRID: AB_955447
Bacterial and virus strains		
AAV2/9-sGFAP (GfaABC1D)-mCherry	WZ Bioscience	AV200088

(*Continued on next page*)

Please cite this article in press as: Luan et al., A reciprocal glial circuit calibrates injury information and governs the tissue response balance, Neuron (2026), https://doi.org/10.1016/j.neuron.2026.03.031

Continued

REAGENT or RESOURCE	SOURCE	IDENTIFIER
AAV2/9-sGFAP (GfaABC1D)-$hM_3D(Gq)$-mCherry	WZ Bioscience	AV202006
AAV2/9-sGFAP (GfaABC1D)-$hM_3D(Gq)$	This paper	N/A
AAV2/9-sGFAP (GfaABC1D)-Cre	WZ Bioscience	AV204012
AAV2/9-sGFAP (GfaABC1D)-GCaMP6f	BrainVTA	PT-2560
AAV2/9-sGFAP (GfaABC1D)-NES-jRGECO1a	BrainVTA	PT-1860
AAV2/9-sGFAP (GfaABC1D)-Cas9-U6-sgRNA-CNAα	This paper	N/A
AAV2/9-sGFAP (GfaABC1D)-Cas9-U6-Scrambled-sgRNA	This paper	N/A
AAV2/9-sGFAP (GfaABC1D)-Cas9-U6-sgRNA-Panx1	This paper	N/A
AAV2/9-sGFAP (GfaABC1D)-Panx1	This paper	N/A
AAV2/9-sGFAP (GfaABC1D)-ATP1.0	This paper	N/A
Chemicals, peptides, and recombinant proteins		
Avertin	Sigma-Aldrich	T48402; CAS: 75-80-9
RIPA buffer	Beyotime	P0013B
Triton X-100	Sigma-Aldrich	X100; CAS: 9036-19-5
PBS	Solarbio	P1010; CAS: 12111-21-6
Tween-20	Solarbio	T8220; CAS: 9005-64-5
4% Paraformaldehyde	Solarbio	P1110; CAS: 30525-89-4
Fetal Bovine Serum	Gibco	A2743112CP; CAS: 9014-81-7
Normal Donkey Serum	Jackson ImmunoResearch Labs	017-000-121
Probenecid	Invitrogen™	P36400; CAS: 57-66-9
IL-1beta Neutralizing antibody	R&D Systems	AF-401-NA
IL-1beta protein, Mouse	MCE	HY-P7073
TNF-alpha/TNFSF2 Protein, Mouse (156a.a)	MCE	HY-P7090
IL-1 alpha Protein, Mouse	MCE	HY-P7072
IL-6 Protein, Mouse	MCE	HY-P7063
C1q Protein, Mouse	MCE	HY-NP0194A
MCP-1/CCL2 Protein, Mouse	MCE	HY-P7764
MIP-1 alpha/CCL3 Protein, Mouse (His)	MCE	HY-P7768
IL-1RA/IL-1RN Protein, Mouse	MCE	HY-P72566
Raleukin/Anakinra	MCE	HY-108841; CAS: 143090-92-0
Clozapine N-oxide	MCE	HY-P7090; CAS: 34233-69-7
Tamoxifen	MCE	HY-13757A; CAS: 10540-29-1
BLZ945	MCE	HY-12768; CAS: 953769-46-5
Deschloroclozapine	MCE	HY-42110; CAS: 1977-07-7
Cyclosporin A	MCE	HY-B0579; CAS: 59865-13-3
Tacrolimus	MCE	HY-13756; CAS: 104987-11-3
AMG-9810	MCE	HY-101736; CAS: 545395-94-6
HC-067047	MCE	HY-100208; CAS: 883031-03-6
Zegocractin	MCE	HY-101942; CAS: 1713240-67-5
2-Aminoethyl diphenylborinate	MCE	HY-W009724; CAS: 524-95-8
Thapsigargin	MCE	HY-13433; CAS: 67526-95-8
Cytarabine hydrochloride	MCE	HY-13605A; CAS: 69-74-9
Critical commercial assays		
Mouse IL-1β ELISA Kit	QuantiCyto	EMC001b.96

(*Continued on next page*)

Please cite this article in press as: Luan et al., A reciprocal glial circuit calibrates injury information and governs the tissue response balance, Neuron (2026), https://doi.org/10.1016/j.neuron.2026.03.031

Continued

REAGENT or RESOURCE	SOURCE	IDENTIFIER
BCA protein assay kit	Biomed	PA101-01
One Step TUNEL Apoptosis Assay Kit	Beyotime	C1090
Nissl Stain Kit (Cresyl Violet Method)	Solarbio	G1430
Super ECL Detection Reagent	Thermo Scientific™	34580
Deposited data		
BulkRNA-seq raw data	This paper	SRA: # PRJNA1396901
Code	This paper	Zenodo; doi: 10.5281/zenodo.19107777
Experimental models: Organisms/strains		
Mouse: C57BL/6J	Jackson Laboratory	RRID: IMSR_JAX:000664
Mouse: C57BL/6JGpt -Panx1^{em1Cflox}/Gpt (*Panx1*$^{fl/fl}$)	GemPharmatech	T008074
Mouse: B6.129P2(Cg)-Cx3cr1tm1Litt/J (*CX3CR1*-GFP)	Jackson Laboratory	RRID: IMSR_JAX:005582
Mouse: *P2ry12*$^{-/-}$	Gene Manipulation Core, CIBR	N/A
Mouse: B6.129P2(Cg)-Cx3cr1tm2.1 (cre/ERT2) Litt/WganJ (*Cx3cr1*-CreERT)	Jackson Laboratory	RRID: IMSR_JAX:021160
Mouse: B6N;129-Tg (CAG-CHRM3*,-mCitrine)1Ute/J	Jackson Laboratory	RRID: IMSR_JAX:026220
Mouse: R26-LSL-mScarletX3	Genetic Manipulation Core, CIBR	N/A
Mouse: C57BL/6JGpt-Il1bem1Cflox/Gpt (*Il1b*$^{fl/fl}$)	GemPharmatech	T007839
Mouse: B6.129(Cg)-Il1r1tm1.1Rbl/J (*Il1r1*$^{fl/fl}$)	Jackson Laboratory	RRID: IMSR_JAX:028398
Mouse: C57BL/6J-Tg (Thy1-GCaMP6f) GP5.17Dkim/J	Jackson Laboratory	RRID: IMSR_JAX:025393
Mouse: C57BL/6NCya-Entpd1em1/Cya (CD39$^{-/-}$)	Cyagen	S-KO-01408
Mouse: B6.129S1-Nt5etm1Lft/J (CD73$^{-/-}$)	Jackson Laboratory	RRID: IMSR_JAX:018986
Mouse: C57BL/6-Tmem119em1 (cre/ERT2) Gfng/J (*TMEM119*-CreERT)	Jackson Laboratory	RRID: IMSR_JAX:031820
Mouse: *Aldh1l1*-CreERT2	Laboratory Animal Resource Center, CIBR	N/A
Mouse: C57BL/6JGpt-P2ry12em1Cflox/Gpt (*P2Y12*$^{fl/fl}$)	GemPharmatech	T006628
Oligonucleotides		
sgRNA targeting sequence: CNAα #1: F-CACCGGGGTGCTTC GATTCTCCGAC	This paper	N/A
sgRNA targeting sequence: CNAα #1: R- AAACGTCGGAGAATCGAAGCACCCC	This paper	N/A
sgRNA targeting sequence: CNAα #2: F-CACCGTAATGATGGGAAACCTCGTG	This paper	N/A
sgRNA targeting sequence: CNAα #2: R-AAACCACGAGGTTTCCCATCATTAC	This paper	N/A
sgRNA targeting sequence: CNAα #3: F-CACCGAAGTCACCGGCTGACAGCAA	This paper	N/A
sgRNA targeting sequence: CNAα #3: R-AAACTTGCTGTCAGCCGGTGACTTC	This paper	N/A
sgRNA targeting sequence: Panx1 #1: F-CACCGCCACTTCAAGTACCCAATCG	This paper	N/A

(*Continued on next page*)

Please cite this article in press as: Luan et al., A reciprocal glial circuit calibrates injury information and governs the tissue response balance, Neuron (2026), https://doi.org/10.1016/j.neuron.2026.03.031

Continued

REAGENT or RESOURCE	SOURCE	IDENTIFIER
sgRNA targeting sequence: Panx1 #1: R-AAACCGATTGGGTACTTGAAGTGGC	This paper	N/A
sgRNA targeting sequence: Panx1 #2 F-CACCGGAAGAACGTGTAGACGACCA	This paper	N/A
sgRNA targeting sequence: Panx1 #2 R-AAACTGGTCGTCTACACGTTCTTCC	This paper	N/A
sgRNA targeting sequence: Panx1 #3 F-CACCGGTCCGAGAACACATACTCCG	This paper	N/A
sgRNA targeting sequence: Panx1 #3 R-AAACCGGAGTATGTGTTCTCGGACC	This paper	N/A
sgRNA targeting sequence: Scramble #1: F-CACCGACTCTGCGGTGTCGCGTACT	This paper	N/A
sgRNA targeting sequence: Scramble #1: R-AAACAGTACGCGACACCGCAGAGTC	This paper	N/A
sgRNA targeting sequence: Scramble #2: F-CACCGGTGACGAACTGTTATGGCAA	This paper	N/A
sgRNA targeting sequence: Scramble #2: R- AAACTTGCCATAACAGTTCGTCACC	This paper	N/A
sgRNA targeting sequence: Scramble #3: F-CACCGGCAATCGGCAGAACTCAACG	This paper	N/A
sgRNA targeting sequence: Scramble #3: R- AAACCGTTGAGTTCTGCCGATTGCC	This paper	N/A
Recombinant DNA		
pAAV-sGFAP (GfaABC1D)-Cas9-U6-sgRNA-CNAα	This paper	N/A
pAAV2/9-sGFAP (GfaABC1D)-Cas9-U6-Scrambled-sgRNA	This paper	N/A
pAAV2/9-sGFAP (GfaABC1D)-Cas9-U6-sgRNA-Panx1	This paper	N/A
Software and algorithms		
Origin2018	OriginLab	https://www.originlab.com; RRID: SCR_014212
ImageJ	NIH	https://imagej.nih.gov/ij/; RRID: SCR_003070
MATLAB R2022a	MathWorks	https://www.mathworks.com/; RRID: SCR_001622
Imaris 10.1	Bitplane	http://www.bitplane.com; RRID:SCR_007370
Adobe photoshop 2022	Adobe	https://www.adobe.com.
AQuA1.0	Wang et al.[43]	https://github.com/yu-lab-vt/AQuA.

EXPERIMENTAL MODEL AND STUDY PARTICIPANT DETAILS

Animals

All animal surgery and experimentation procedures were performed according to protocols approved by the Animal Care & Use Committees of the Chinese Institute for Brain Research (#CIBR-IACUC 007) and the Hungarian Institute of Experimental Medicine. Both male and female mice aged 5–7 weeks were used for *in vivo* surgery and two-photon imaging, while mice aged 2–3 weeks were used for acute brain slices. All mice were either family-housed or pair-housed in a temperature-controlled room with a 12-h light-dark cycle. Animals were randomly assigned to treatment groups, and experiments and analyses were performed blinded to treatment assignments.

Viruses

AAVs were purchased from WZ Bioscience, BrainVTA or packaged from Vector Core at CIBR. All AAVs were aliquoted and stored at −80°C until use.

Please cite this article in press as: Luan et al., A reciprocal glial circuit calibrates injury information and governs the tissue response balance, Neuron (2026), https://doi.org/10.1016/j.neuron.2026.03.031

METHOD DETAILS

Stereotaxic surgery and virus injection

For *in vivo* two-photon imaging, mice were anesthetized with an intraperitoneal (i.p.) injection of avertin (250 mg/kg of body weight), and a metal head-fixed recording chamber was affixed to the skull. After 3-4 days of recovery, mice were re-anesthetized and placed on a stereotaxic frame (RWD Instruments). A cranial window was opened on the visual cortex, followed by the injection of 500 nL of AAV into the cortex (coordinates: AP: -2.2 mm relative to Bregma, ML: 2.0 mm relative to midline, and DV: 0.65 mm below the dura, with an angle of 30°) using a microsyringe pump (Nanoliter 2000 injector, WPI) at a slow rate of 60 nL/min. For imaging with an enlarged field of view, AAVs were injected at four different positions (each 500 nL). After the injection was completed, the glass electrode was left for an additional 5 minutes before slowly withdrawing. After cleaning with sterile saline, a 4 mm × 4 mm coverslip was used to replace the skull. Mice were recovered from anesthesia under a heat pad. In some experiments the thinned-skull cranial window was used after 2 weeks of viral infection, with a similar protocol described before.[44] For acute brain slice experiments, neonatal P3 mice were anesthetized on a pre-cooled metal block and injected with 500 nL AAV into the visual cortex. The tissue glue was used to stick the skin and mice were returned to their home cage after fully recovering from anesthesia.

Acute brain slice preparation

To prepare acute brain slice, mice were anesthetized with avertin after two weeks of viral injection, and were transcranial perfused with 10 mL pre-cooled slicing buffer containing 110 mM choline-Cl, 2.5 mM KCl, 1.25 mM NaH_2PO_4, 25 mM $NaHCO_3$, 7 mM $MgCl_2$, 25 mM glucose, and 0.5 mM $CaCl_2$. The mice were then decapitated, and brains were immediately removed and placed in pre-cooled oxygenated slicing buffer (oxygenated with 95% O_2 + 5% CO_2). The brains were sectioned into 250 μm slices using a VT1200 vibratome (Leica), and the slices containing the visual cortex were immediately transferred to oxygenated ACSF containing 125 mM NaCl, 2.5 mM KCl, 1.25 mM NaH_2PO_4, 25 mM $NaHCO_3$, 1.3 mM $MgCl_2$, 25 mM glucose, and 2 mM $CaCl_2$. Ca^{2+}-free ACSF was prepared by omitting $CaCl_2$ and adding 0.1 mM EDTA. Slices were recovered at 33°C for 30 minutes before being transferred to a chamber for imaging.

Microglia depletion and repopulation

For microglia depletion, the CSF1R inhibitor BLZ945 (MCE, HY-12768) was added into food pellets at a concentration of 2 g/kg, and mice were fed 3 g of the pellets twice daily for 14 consecutive days. For microglia repopulation, BLZ945-containing food was replaced with standard chow to allow microglial repopulation over the next 14 days in previously microglia-depleted mice.

Two-photon imaging and focal laser ablation (FLA)

In vivo imaging of awake mice and acute brain slices was conducted using a two-photon laser-scanning microscope (FVMPE-RS; Olympus) equipped with a pulsed Ti:sapphire laser (Insight Deep See; Newport Spectra-Physics). Images were acquired using a 25X water immersion objective (XLPLN25XWMP2, 1.05 NA, Olympus). For imaging ATP dynamics using GRAB-ATP1.0 sensors,[45] the recording frequency was set at 10 Hz, and every 10 images were averaged. Each recording episode typically lasted for 20 minutes *in vivo* and 10 minutes in acute slices. The imaging field was typically 500 μm × 500 μm. For Ca^{2+} imaging using Thy1-GCaMP6f mice, the recording frequency was set at 7.5 Hz, each recording episode was 10 minutes.

For generating FLA, the 920 nm laser was set at its maximum power and scanned the center of the imaging region (50 μm in diameter) for 2 sec using the Tornado scanning mode. Successful FLA could be observed by the formation of a high fluorescence circle around the FLA region. For generating FLA with different intensities, the laser power and duration was adjusted (weak: 40% laser power for 0.4 s; intensive: 100% laser power for 2 s). In slice experiments, the FLA protocol was set as 100% laser power for 1 s. In experiments related to IL-1β detection and gene expression profiling, an extended FLA was performed in which multi-regions of 50 μm in diameter was injured to assess the outcome at tissue level.

For the DCZ treatment in MicroDREADD mice, experiments were performed on a Femto2D-DualScanhead microscope (Femtonics Ltd., Budapest, Hungary) coupled with a Chameleon Discovery laser (Coherent, Santa Clara, USA). The wavelength of the laser was set to 920 nm to measure the ATP signals. Following excitation, the fluorescent signal was collected using a Nikon 18X water immersion objective. Data acquisition was performed by MESc software (Femtonics Ltd.). The recording frequency was set at 30 Hz. A 100 μL solution of 5 μg/kg DCZ (MCE, # HY-42110) was used.

Traumatic brain injury

The traumatic brain injury model was established as previously described.[46,47] Briefly, male C57BL/6J mice and *Cx3cr1*-CreERT-*Il1b*$^{flox/flox}$ mice were randomly assigned, and were positioned in a stereotaxic frame. Traumatic brain injury was induced using a gravity-driven impact device (Cranial and spinal cord impactor, Hengqinda Ltd.) with a 40 g weight dropped from a height of 5 cm and an impactor tip diameter of 0.5 mm. Mice were sacrificed at 1 and 7-days post-injury, and brains were collected for immunostaining.

Measurement of ATP levels in cell cultures

Primary astrocytes were isolated from neonatal (P1) mouse brains and cultured in MEM supplemented with 10% fetal bovine serum and 40 μg/ml gentamycin.[48] Microglia were isolated from mixed glial cultures by mild trypsinization at 21–28 days *in vitro*. For co-culture

Please cite this article in press as: Luan et al., A reciprocal glial circuit calibrates injury information and governs the tissue response balance, Neuron (2026), https://doi.org/10.1016/j.neuron.2026.03.031

experiments, microglia were added to astrocyte cultures at a defined ratio and maintained in astrocyte culture medium until ATP activity detection. To assess ATP dynamics, astroglia cultures were infected with the GRAB-ATP1.0 sensor. Fluorescence intensity was measured with a multimode plate reader (Cytation 5, BioTek) over 30-minute periods at 5-minute intervals, after 8 or 24 hours of vehicle or IL-1β (50 ng/ml) treatment. For kinetic monitoring of ATP release into the cell culture media, we used the RealTime-Glo™ Extracellular ATP Bioluminescent Assay (Promega), according to the manufacturer's instructions. Data were acquired every 100 seconds with an 8-second integration time using a Cytation 5 plate reader, either over a 30-minute time window 24 hours after IL-1β (50 ng/ml) treatment of astrocytes or over a 10-20 h time window in astroglia versus astroglia/microglia co-cultures.

Drug administration

IL-1β (200 ng/mice) was prepared in saline and administered by i.p. injection, 60 minutes before *in vivo* imaging or FLA stimulation. Pannexin blocker probenecid (PBN, 4 mg/ml) was also administered by i.p. injection at a concentration of 200 mg/kg, 6 hours before *in vivo* imaging or FLA stimulation. Anakinra (10 mg/kg) was prepared in saline and administered by i.p. injection, 60 minutes before *in vivo* imaging or FLA stimulation. To induce Cre recombinase function in CreERT transgenic mice, tamoxifen was added to the food palate at a concentration of 100 mg/kg, and mice were given the food every day for 21 consecutive days.

Secreted IL-1β protein detection

Visual cortex tissues were isolated from mice subjected to multi-region FLA injury at various time points (-0.5 h, 0.5 h, and 6 h post-injury). The brain tissues were gently homogenized on ice using a glass homogenizer in cold PBS buffer to extract secreted IL-1β protein. The homogenate was first centrifuged at low speed (500g for 10 minutes) to pellet debris, and the resulting supernatant was then subjected to high-speed centrifugation (10,000g for 10 minutes) to obtain a clarified supernatant. Secreted IL-1β levels were quantified using an enzyme-linked immunosorbent assay (ELISA) according to the manufacturer's instructions.

Cell apoptosis detection

Mice were sacrificed at the designated time points and transcardially perfused with ice-cold phosphate-buffered saline (PBS) followed by 4% paraformaldehyde (PFA) in PBS. Brains were carefully removed, post-fixed in 4% PFA at 4°C for 3 hours, and then cryoprotected in 30% sucrose in PBS until the tissue sank. Brains were embedded in optimal cutting temperature (OCT) compound and frozen at –80°C. Coronal brain sections (40 μm) were cut on a cryostat and mounted onto glass slides. Apoptotic cells were detected using the TUNEL assay according to the manufacturer's instructions. Briefly, sections were rinsed with PBS, permeabilized with 0.5% Triton X-100 in PBS for 10 minutes, and incubated with TUNEL reaction mixture in a humidified chamber at 37°C for 1 hour. Sections were washed with PBS, counterstained with DAPI, and mounted with anti-fade mounting medium. Stained sections were imaged using a fluorescence microscope, and TUNEL-positive cells were quantified in defined regions of interest.

Nissl staining

Fresh brain tissues were fixed in 4% PFA and cryoprotected in a series of 30% sucrose solutions in PBS until the tissue sank and embed in OCT compound. Tissues were sectioned into 40 μm slices and were soaked in distilled water. Sections were then immersed in Cresyl Violet and incubated at 56°C for 5 min. Sections were differentiated in Nissl differentiation solution for less than 2 mins, and dehydrated in absolute ethanol and xylene before imaging.

Immunofluorescence staining and Western blot

Mice were anesthetized and transcranial perfused with saline, followed with 4% paraformaldehyde (PFA) in PBS. The brains were postfixed in 4% PFA at 4°C overnight, and then transferred to 30% sucrose/PBS at 4°C for 24∼48 hrs. Brains were sectioned on a freezing microtome (Leica, CM3050S), coronal sections (50 μm) of the visual cortex were collected. For immunofluorescence (IF) of fixed mouse brain, sections were permeabilized with 0.5% Triton X-100 (Sigma-Aldrich, #X100) in PBS, blocked with blocking buffer (5% BSA, 0.3% Triton-X100 in PBS) at room temperature for 1 hr, and then incubated with primary antibodies in antibody dilution buffer (1% BSA, 0.3% Triton-X100 in PBS) in a humidified chamber at 4°C overnight. The sections were then stained with secondary antibodies (1:1000 in antibody dilution buffer) at room temperature for 2 hrs, then mounted with DAPI (Sigma-Aldrich, #D9542) in glycerol/PBS (1:1) (0.1 μg/ml) on coverslips. Immunofluorescence was acquired using a Nikon Eclipse Ti-E inverted microscope (Nikon Instruments Europe B.V., Amsterdam, The Netherlands), with a CFI Plan Apochromat VC 60X oil immersion objective (numerical aperture: 1.4) and an A1R laser confocal system with 405, 488, 561 and 647 nm lasers (CVI Melles Griot). Scanning was done in line serial mode, and pixel size was 100 x 100 nm. Z stack images (40 μm) of IF samples were obtained using a laser scanning confocal microscope (Leica TCS SP8) and analyzed with Imaris software (Oxford Instruments, version 10.1).

For the staining of CD11c-positive cells, confocal image stacks with double immunofluorescent labeling (microglia and CD11c) were acquired from the somatosensory cortex of CX3CR1^{+}/GFP (IMSR_JAX:005582) mice. Sections were mounted on glass slides, and coverslipped with Aqua-Poly/Mount (Polysciences). Images were analyzed using an unbiased, semi-automated method. All labeled and identified cells were counted, when the whole cell body was located within the Z-stack. Regions of interest (ROIs) of

Please cite this article in press as: Luan et al., A reciprocal glial circuit calibrates injury information and governs the tissue response balance, Neuron (2026), https://doi.org/10.1016/j.neuron.2026.03.031

105 × 105 × 35 μm were defined. Within each ROI, all *CX3CR1*-GFP and DAPI-positive cells were first identified, after which the proportion of CD11c-positive cells within this population was determined. For the lesioned samples, ROIs were defined within the injured area, at a distance of no more than 400 μm from the border of the intact tissue.

For Western blot experiments, brain slices were homogenized on ice in RIPA lysis buffer (Beyotime, #P0013B) supplemented with a protease inhibitor cocktail (Thermo Scientific™, #78429) to extract total protein. Protein concentration was determined using a BCA protein assay kit (Biomed, #PA101-01). Approximately 50 μg of total protein was separated by SDS-PAGE and transferred onto PVDF membranes (Millipore, IPVH00010). Membranes were blocked with 5% BSA in TBS containing 0.1% Tween-20 and incubated overnight at 4°C with primary antibodies. Subsequently, membranes were incubated with secondary antibodies at room temperature for 1 hour. Protein bands were detected using the Super ECL Detection Reagent (Thermo Scientific™, #34580) and visualized with an Invitrogen Chemiluminescent Imaging System (Invitrogen). Band intensities were quantified using ImageJ software (NIH).

Gene expression profiling

For Bulk RNA sequencing, brain samples were dissected and the extracted RNA was send to Novogene (Beijing) for subsequent steps. RNA integrity was assessed using the RNA Nano 6000 Assay Kit of the Bioanalyzer 2100 system (Agilent Technologies, CA, USA). A total amount of 1 μg RNA per sample was used as input material. Poly-T oligo-attached magnetic beads were used to collect purified mRNA. First strand cDNA was synthesized using random hexamer primer and M-MuLV Reverse Transcriptase (RNase H). Second strand cDNA synthesis was performed subsequently using DNA Polymerase I and RNase H. The remaining overhangs were converted to blunt ends using exonuclease/polymerase activities. Adaptors with a hairpin loop structure were ligated to prepare for hybridization after adenylation of 3' ends of DNA fragments. To selectively choose 370∼420 bp cDNA fragments, the library fragments were purified by the AMPure XP system (Beckman Coulter, Beverly, USA), followed by PCR. Finally, PCR products were purified with the AMPure XP system, and library quality was evaluated using the Agilent Bioanalyzer 2100 system. Following the manufacturer's instructions, the index-coded samples were clustered on a cBot Cluster Generation System using TruSeq PE Cluster Kit v3-cBot-HS (Illumina). After cluster generation, the library preparations were sequenced on Illumina Novaseq platform, generating 150 bp paired-end reads.

Visual stimulation

Thy1-GCaMP6f mice were injected with AAVs to express either astrocyte-specific calcineurin A-α sgRNA or scrambled sgRNA for 4 weeks. Prior to visual stimulation, mice were acclimated in the two-photon imaging environment for 60 minutes under dark conditions. Visual stimuli were generated using MATLAB. For widefield visual stimulation, stimuli were presented on a secondary computer monitor (35 × 25 cm, 1920 × 1080 pixels, 60 Hz refresh rate) positioned 20 cm from the mouse's eye at a 30° angle to the right of the midline. The visual stimuli consisted of a moving bar with a constant speed (0.007 cycles/degree spatial frequency; 13 Hz temporal frequency) sweeping across the mouse's visual field in one direction. Each stimulus lasted 5 seconds, followed by a 2-minute interval, and was repeated for 3 times. Fluorescence changes ($\Delta F/F_0$) were measured with the average fluorescence signal of baseline as F_0. Neurons were considered responsive to visual stimuli if their stimulus-evoked $\Delta F/F_0$ exceeded 20%.[49]

Data analysis

To identify Inflare ROIs, all *in vivo* and acute slice imaging data were processed using AQuA1.0 software in MATLAB.[43] Regions with significant fluorescence changes were identified using the flowing parameters: Intensity threshold scaling factor, 3.1; Smoothing (sigma), 0.5; Minimum size (pixels), 50; Temporal cut threshold, 5; Growing z threshold, 1; Rising time uncertainty, 8; Propagation smoothness, 2; Z score threshold, 2; Maximum distance, 5; Maximum correlation, 5; Maximum time difference, 5; Temporally extend events, Ture; Ignore delay Tau, False. Identified regions were further validated manually.

The Microglial Feedback Index (MFI) was defined as the relative difference of injury-evoked changes in Inflare numbers (ΔInflares) between microglia intact (+mic) and microglia depleted (-mic) conditions.

$$\mathrm{MFI} = \frac{[\Delta\mathrm{Inflare}(-\mathrm{mic}) - \Delta\mathrm{Inflare}(+\mathrm{mic})]}{\Delta\mathrm{Inflare}(+\mathrm{mic})}.$$

For cell morphology reconstruction and analysis, the number of neurons, microglia, astrocyte and apoptosis cells were evaluated using the spot function based on NeuN, IBA1, GFAP positive cells in Imaris software. To quantify microglia morphology, the length of processes, terminal points of branches, intersections of distance from the soma center and soma volume were measured based on IBA1 staining, using the filament and surface function in Imaris 10.1.

QUANTIFICATION AND STATISTICAL ANALYSIS

All summary data were presented as the mean ± s.e.m unless otherwise specified, with error bars represented the s.e.m. Pearson's omnibus normality test was used to evaluate the normality and equality of variances between groups. For paired groups,

Please cite this article in press as: Luan et al., A reciprocal glial circuit calibrates injury information and governs the tissue response balance, Neuron (2026), https://doi.org/10.1016/j.neuron.2026.03.031

the statistic difference was determined using paired Student's t-test. For unpaired groups, F-test was first performed to compare the variance, followed by Student's t-test. Mann-Whitney U test was performed to compare differences between two independent groups when the dependent variable is either ordinal or continuous, but not normally distributed. The Kolmogorov-Smirnov test compares whether the distributions of two samples are the same. $P > 0.05$ was set as no significance (n.s.), while $p < 0.05$ was marked as *, $p < 0.01$ with **, and $p < 0.001$ as ***, all statistical tests were two-sided. All statistical details for the main and supplementary figures are provided in Table S1.